

ABSTRACT

BOHON, STEVEN ROBERT. Performance and Emissions Testing of a Bi-Fuel Outboard Spark-Ignition Engine (under the direction of Tiegang Fang).

With the increasing concern about the future availability of gasoline and continuously stringent engine emissions regulatory standards, the need for an alternative to gasoline as a primary engine fuel is becoming increasingly important. One proposed alternative is to use natural gas due to its availability, low cost, and generally reduced engine emissions. However, due to volumetric efficiency losses, the conversion of a standard spark-ignition engine originally operating on gasoline to run on natural gas has been shown to produce considerable power reductions. Additionally, improperly tuned natural gas conversion kits could potentially increase certain emissions quantities compared to gasoline. This work reports the results of an experiment designed to characterize the performance and emissions of a commonly used gasoline outboard boat motor converted to run on natural gas. Reported are the comparisons between gasoline and natural gas for widely used engine operating parameters for gauging engine performance related to power output and harmful emissions, including oxides of nitrogen, unburned hydrocarbons, and carbon monoxide, for comparison of the two test fuels. Results indicate that operation on natural gas greatly reduces harmful hydrocarbon and carbon monoxide emissions at the cost of reduced engine power output and potentially increased oxides of nitrogen emissions.

Performance and Emissions Testing of a Bi-Fuel Outboard Spark-Ignition Engine

by
Steven Robert Bohon

A thesis submitted to the Graduate Faculty of
North Carolina State University
in partial fulfillment of the
requirements for the Degree of
Master of Science

Mechanical Engineering

Raleigh, North Carolina

2014

APPROVED BY:

Dr. Tarek Echehki
Member of Advisory Committee

Dr. Alexei Saveliev
Member of Advisory Committee

Dr. Tiegang Fang
Chair of Advisory Committee

DEDICATION

This thesis is dedicated to my father, Bruce Bohon, for all of his wisdom and guidance, to my mother, Sandy Bohon, for all of her encouragement and love, and especially to my brother, Myles Bohon, as he has served as an example for me throughout my life.

BIOGRAPHY

The author was born Steven Robert Bohon to Bruce and Sandy Bohon on June 27th, 1989 in Dallas, Texas. After moving two years after his birth, Steven spent his early elementary years in Kokomo, Indiana. In third grade, Steven moved to High Point, North Carolina and completed his elementary, middle, and high school education. While in high school, Steven developed a passion for music and continues to play guitar and mandolin today. Steven began to pursue a taste for design and mechanical systems towards the end of his high school career and enrolled in North Carolina State University to major in Mechanical Engineering. Steven developed an interest in internal combustion engine research while taking an introductory course with Dr. Tiegang Fang. Steven graduated Magna Cum Laude in 2012 and continued schooling in a pursuit of a Master's degree of Mechanical Engineering at North Carolina State University. After receiving an opportunity in alternative fuel research, Steven began work under the supervision of Dr. Fang on converted gasoline outboard boat motors to run on natural gas.

ACKNOWLEDGMENTS

The author would first like to acknowledge his advisor Dr. Tiegang Fang for his continued guidance and mentorship throughout this work. The author would also like to thank the members of his advisory committee Dr. Tarek Echehki and Dr. Alexei Saveliev for their support and guidance in the completion of this work. The author would like to thank the sponsor, Blue Gas Marine, Inc., for their funding and support throughout the project. The author would also like to personally thank Dolanimi Ogunkoya, Brian McCann, Myles Bohon, Keeshan Ganatra, Dan Goslen, and Dan Owens. Each of these individuals selflessly gave their time and effort, and without whom this work would have not been possible.

Additionally, the author would like to thank his friends and family for their continued support and guidance. He would like to thank them for being patient with his frustrations and long hours of work at, sometimes, inconvenient times. Without their continued support and understanding, none of this would have been possible.

TABLE OF CONTENTS

LIST OF TABLESvi
LIST OF FIGURES vii
1 INTRODUCTION1
2 EXPERIMENT DESIGN AND SETUP12
 2.1 Dynamometer Set-up..... 13
 2.2 Engine Cooling and Exhaust Removal 20
 2.3 Exhaust Measurement..... 29
 2.4 Fuel Storage and Flow Measurement 31
 2.5 Data Acquisition and Display 37
3 RESULTS42
 3.1 Engine Performance..... 42
 3.2 Major Exhaust Emissions..... 46
 3.3 Fuel Consumption, Fuel Conversion Efficiency, and Flame Temperature..... 52
 3.4 Pollutant Exhaust Emissions 59
4 CONCLUSIONS80
6 REFERENCES84
APPENDIX87

LIST OF TABLES

Table 1 - Engine Specifications	12
Table 2 - Dynamometer minimum feed water pump requirements	17
Table 3 - Hazardous gas alarm thresholds	28
Table 4 - Exhaust gas analyzer measured gases and ranges	29
Table 5 - Assumed natural gas composition.....	46
Table 6 - Assumed heating values	53

LIST OF FIGURES

Figure 1 - Price comparison of natural gas and conventional gasoline from Nov. 2012 to Nov. 2013	3
Figure 2 - Dynamometer feed water system.....	14
Figure 3 - Land-and-Sea water-brake absorber	15
Figure 4 - Water-brake absorber mounting configuration.....	16
Figure 5 - Wayne 1.5 hp main feed water supply pump	18
Figure 6 - Automated load control valve.....	19
Figure 7 - Fan and radiator system with reservoir cooling pump.....	20
Figure 8 - Engine-cooling tank and exhaust shroud	22
Figure 9 - Exhaust port location (left) and exhaust port close-up (right)	23
Figure 10 - Exhaust suction tubing.....	24
Figure 11 - Exhaust removal blower	24
Figure 12 - Engine cooling-tank insertion point with dynamometer absorber hook-ups	26
Figure 13 - Hazardous gas alarm	28
Figure 14 - Custom sample probe	30
Figure 15 - Inserted sample probe configuration	31
Figure 16 - CNG tank in enclosure.....	32
Figure 17 - CNG tank refueling and delivery high-pressure valve and tubing configuration	33
Figure 18 - CNG pressure reducer and electro-valve system.....	34
Figure 19 - Reducer warming water supply pump	35
Figure 20 - Teledyne series 200 mass flow meter	36

Figure 21 - Gasoline tank and scale mass flow measurement configuration	37
Figure 22 - Experimental data acquisition configuration	38
Figure 23 - Land-and-Sea data computer and controller	39
Figure 24 - Mass flow meter power supply with digital display and exhaust gas analyzer	40
Figure 25 - Desktop computer with DYNO-Max Pro console display	41
Figure 26 - SAE corrected brake torque for over swept engine speeds	43
Figure 27 - SAE corrected brake power output over swept engine speeds	45
Figure 28 - Measured CO, CO ₂ , and O ₂ concentrations for gasoline	48
Figure 29 - Measured CO, CO ₂ , and O ₂ concentrations for natural gas	49
Figure 30 - CO comparison	50
Figure 31 - CO ₂ comparison	51
Figure 32 - O ₂ comparison.....	52
Figure 33 - Gasoline bsfc contour map	54
Figure 34 - Natural gas bsfc contour map	55
Figure 35 - Test fuel bsfc comparison	56
Figure 36 - Fuel conversion efficiency comparison	57
Figure 37 - Adiabatic flame temperature over equivalence ratio (K).....	59
Figure 38 - Gasoline specific HC emissions contour map	61
Figure 39 - Gasoline HC emissions index contour map.....	61
Figure 40 - Gasoline measured HC concentrations contour map.....	62
Figure 41 - Natural gas specific HC emissions contour map	63
Figure 42 - Natural gas HC emissions index contour map.....	64

Figure 43 - Natural gas measured HC concentrations contour map.....	64
Figure 44 - Gasoline specific CO emissions contour map	66
Figure 45 - Gasoline CO emissions index contour map.....	67
Figure 46 - Gasoline measured CO concentrations contour map.....	67
Figure 47 - Natural gas specific CO emissions contour map	69
Figure 48 - Natural gas CO emissions index contour map.....	69
Figure 49 - Natural gas measured CO concentrations contour map.....	70
Figure 50 - Gasoline specific NO _x emissions contour map	72
Figure 51 - Gasoline NO _x emissions index contour map.....	72
Figure 52 - Gasoline measured NO _x concentrations contour map.....	73
Figure 53 - Natural gas specific NO _x emissions contour map	74
Figure 54 - Natural gas NO _x emissions index contour map.....	74
Figure 55 - Natural gas measured NO _x concentrations contour map.....	75
Figure 56 – HC specific emissions (left) and emissions index (right) comparisons at 2500 rpm.....	78
Figure 57 - CO specific emissions (left) and emissions index (right) comparisons at 2500 rpm	78
Figure 58 - NO _x specific emissions (left) and emissions index (right) comparisons at 2500 rpm.....	79

1 INTRODUCTION

Concerns for environmental maintenance and the potential future peak and decline of worldwide oil production have vastly increased the necessity for research into cleaner, more abundant energy sources to reduce the share of the world's energy usage that is based on oil. The future supply of oil is a source of current debate with individual studies maintaining that at the current rates of consumption and production, a peak in the world's ability to produce oil will soon be reached and the global demand for oil will struggle to be met [1].

Additionally, carbon based emissions have become a dominating topic of environmental concern and have increased the involvement of governments globally with respect to the choice of primary energy sources. Governmental emissions standards continue to accelerate a need for alternative primary energy sources other than oil through the increasingly stringent emissions requirements enforced in recent years. As these standards continue to increase, the transportation industry is a major driving force for developments in such alternative fuel research in that the continuously increasing emissions requirements and fuel prices demand a viable alternative to oil products like gasoline. Fossil fuels prove to be readily interchangeable [2]. Due to this interchangeability of fossil fuels, extensive research into the replacement of oil with natural gas in the transportation sector continues globally. Large growth opportunities exist for natural gas within the transportation industry in either a direct replacement fuel for current gasoline operated vehicles or indirectly as an energy source for electrical power [2]. As the price of natural gas continues to remain significantly lower than that of oil, natural gas is becoming more utilized throughout the global transportation market, especially as a gasoline alternative in spark ignition (SI) engines.

Economides and Wood [2] indicate that natural gas reserves have been steadily increasing at rates of 5% annually since the 1970s. Concerns about the environmental factors associated with the development of natural gas reserves are still a factor in establishment of natural gas as a primary fuel source in that awareness of water and air pollution potentials related to the shale gas industry [3]. However, natural gas is still thought to play a large role in the transportation sector in the future and maintains many advantages over oil specifically in the availability and price advantage of natural gas compared to oil [3]. Fig. 1, adapted from [4], [5], illustrates the price comparison in dollars per million BTU between natural gas and gasoline over the last year. As seen in the figure, the price of natural gas in terms of energy is consistently more than four times less that of gasoline.

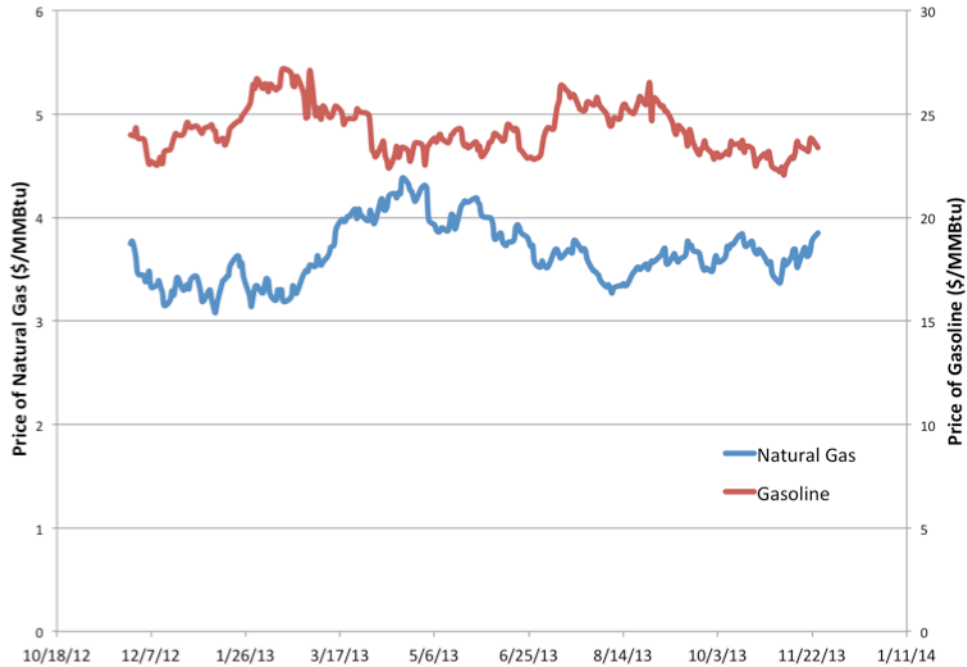


Figure 1 - Price comparison of natural gas and conventional gasoline from Nov. 2012 to Nov. 2013

Brazil has already begun numerous SI engine conversions to natural gas, and Dondero et al. [6] discuss the nation’s experiences with natural gas converted vehicles. According to [6], “The economic advantage of converting a vehicle from gasoline into gas reaches a 65% saving for the final user, due to the price differential between natural gas [and gasoline].” However, the report indicates issues exist in the relatively unregulated aftermarket conversion of SI engines that, while on average reduce CO emissions, can greatly increase HC and NO_x emissions to points often outside of regulation limits, which is in general due to a lack of controlled calibration of the converted engine during the conversion process [6]. Dondero et al. state that while the abundance of the supply of natural gas secure future fuel availability, policies and legislation regarding the potential

environmental impact for improperly tuned, converted engines would need to be developed before a nation could seriously consider the use of natural gas SI engines as an alternative to gasoline [6].

Cho and He [7] completed a review of SI natural gas engines operating at lean and stoichiometric conditions. The review highlights primarily the performance and stability related operating characteristics for running lean burn and stoichiometric natural gas engines as an example of the fuel's potential to reduce hazardous emissions and greenhouse gases from internal combustion engines.

The review begins with an examination of lean burn natural gas engines. According to [7], "...NG engines using high compression ratio, lean burn mixture or high exhaust gas recirculation would be expected to outperform gasoline engines in torque, power and can allow a remarkable reduction in pollutant emissions and an improvement in thermal efficiency." However, as the air-fuel mixture is continually leaned out in order to suppress NO_x emissions, reduced thermal efficiency, engine misfire, incomplete combustion, and, subsequently, higher engine emissions become potentially problematic if valve duration and timing are not optimized [7]. The review also found the fuel economy of lean burn natural gas engines to outperform stoichiometric conditions and determined the engine thermal efficiency depends on a combination of several factors including air-fuel ratio, compression ratio, burning rate, and NO_x emission levels, and thus the authors recognized that to achieve optimal fuel efficiency, these engines should be ran near the lean misfire limits [7]. Due to the relatively low burn velocity of natural gas in air as compared to gasoline in air, the review found that intake methods resulting in increased turbulence levels in the cylinder can reduce

cyclic variability and improve thermal efficiency [7]. Cho and He mention the need for adjusted spark ignition timings to account for flame speed reduction under lean conditions and found that spark advance tends to vary with the natural gas composition and air-fuel ratio in the range between 2° and 10° crank angle more than for gasoline.

The review briefly examines stoichiometric natural gas engines compared to gasoline engines and the lean burn natural gas engine. The authors found that while the NO_x emissions of a stoichiometric natural gas engine with early spark timings are lower than gasoline engines, the thermal efficiency of natural gas at stoichiometric conditions is less than the thermal efficiency of natural gas at lean conditions [7]. Increased fuel economy can be achieved through exhaust gas recirculation (EGR), but the addition of EGR can increase harmful engine emissions [7]. A stoichiometric natural gas engine equipped with EGR and a three-way catalyst reduces the harmful emissions to below emissions regulations and can drastically reduce both NO_x and hydrocarbon emissions compared to the lean burn conditions [7].

The review continues to address additional problems with the general conversion of a gasoline engine to operate on natural gas. Volumetric efficiency of a natural gas engine with port fuel injection can be 10-15% less than that of a port fuel injected gasoline engine and can result in a power loss of over 10% for a natural gas engine compared to an equivalent gasoline engine [7]. Piston, cylinder wall, valve, and valve seat temperatures tend to increase with natural gas, which can result in increased wear rates for the intake valves and seats [7]. Additionally, the lack of detergent additives commonly in gasoline can increase deposit build up and lessen the reliability of engine components in natural gas engines [7]. Finally, the

review recognizes that vehicle driving range and fuel storage for compressed natural gas (CNG) vehicles is limiting in that, for the same energy content, the CNG occupies about four times the volume of gasoline [7].

Korakianitis et al. [8] examined the performance and exhaust emissions of SI and CI engines operating on natural gas. For gasoline SI engines, a key advantage of natural gas over gasoline is the ability to increase the compression ratio of an engine running on natural gas thus increasing the thermal efficiency [8]. However, combining this with other beneficial and negative effects from the conversion process tend to reduce the power output of a gasoline engine converted to run on natural gas around 15% [8]. Korakianitis et al. state that while typical natural gas injection into the intake manifold may result in lower volumetric efficiencies for naturally aspirated engines, turbocharging or supercharging with intercooling can result in power output and thermal efficiency increase in the realm of 50% [8]. In-cylinder direct injection is an alternative to turbocharging or super charging the engine that avoids the volumetric efficiency losses associated with natural gas, but the high-pressure gaseous injectors are currently not available in the open market and direct injection may have an effect on NO_x emissions [8]. For exhaust emissions, changing from gasoline to natural gas will typically reduce the CO emissions significantly and the CO_2 emissions slightly [6], [8]. CO emissions continually decrease from leaner air-fuel mixtures until extremely lean conditions where combustion quality deteriorates and CO and HC emissions drastically increase [7], [8]. Aftermarket conversions of gasoline engines to run on natural gas can increase NO_x emissions up to 170% compared to typical gasoline engine emissions due to higher in-cylinder pressures and temperatures and higher oxygen concentrations from leaner

air-fuel mixtures[6], [8]. However, after successful tuning and additional engine modifications, a natural gas SI engine could result in reduced NO_x, CO, CO₂, and non-methane HC emissions compared to gasoline [8].

For diesel CI engines, additional fuel properties of natural gas must be considered for appropriate engine operation, specifically the cetane number in which natural gas has a significantly lower cetane number than diesel due to natural gas being composed primarily of methane [8]. This leads to ignition difficulties as in that, according to [8], “...in both port-injected and direct-injected natural-gas CI engines, natural gas does not spontaneously ignite under typical CI compression ratios...” In order to control the ignition, a pilot source must be injected using traditional means to act as an ignition source for the natural gas combustion to begin [8]. For dual-fuel operation with natural gas and about 30% of the total fuel energy coming from the pilot fuel, typical port-injection methods of the natural gas can result in only a 2-5% reduction in volumetric efficiency for CI engines [8]. Korakianitis et al. allude to discrepancies between some experimental studies that indicate dual-fuel operation maintains similar thermal efficiencies compared to conventional CI operation and some studies that indicate significantly lower thermal efficiencies, but they conclude that dual-fuel operation depends on the original CI engine and natural gas system used [8]. In regards to emissions, Korakianitis et al. report that dual-fueled CI engines tend to produce significantly less NO_x emission as compared to traditional CI operation, in which the specific reduction amount is dependent largely on the choice of pilot fuel type and quantity [8]. Additional harmful emissions like smoke, soot, and particulate matter are greatly reduced in dual-fuel CI engines, but part-load unburned HC emissions for dual-fuel CI engines are significantly

higher than for traditional CI operation [8]. The addition of EGR can reduce NO_x and HC emissions for the dual-fuel CI engine [8]. As with SI engines, natural gas CI engines benefit from extensive performance and emissions optimizations such as EGR, forced induction, advance spark timing, and catalytic converters to increase power and reduce emissions as compared to conventional CI operation with diesel [8].

Zeng et al. [9] further examine the use of direct injection in a natural gas engine for a range of various fuel injection timings. The study indicates that fuel injection timing strongly influences engine operation especially for late injection timings that did not allow for proper fuel-air mixing, which resulted in high HC emissions [9]. Zeng et al. also found that volumetric efficiency was adversely effected and the equivalence ratio increased as fuel injection timing was advanced [9]. For a constant injection duration, the study concluded fuel injection timing can be optimized for maximum cylinder pressure, rate of pressure rise, and heat release with the shortest combustion durations that maintained minimal levels of HC and CO engine emissions [9].

In an attempt to compare the effect of fuel injection number and location on combustion quality, Shiga et al. [10] utilize a rapid compression machine with a constant compression ratio test different injector and spark plug configurations over a range of stoichiometric to extremely lean combustion mixtures. Direct fuel injection configurations were found to have a relatively insignificant effect on combustion and emission parameters [10]. However, the study found that using stratified injection with optimized injection timings, the lean combustion limit for CNG injection could be greatly reduced to extremely

lean conditions from a fuel-air equivalence ratio of 0.6 for the homogeneous mixture to an equivalence ratio of 0.02 [10].

To address the significant amounts of methane emitted from natural gas engines, Rink et al. [11] examine the performance of alternative purification systems on conversion performance. The purification system design was based on existing designs of a heat-integrated concept revolving around a metallic countercurrent heat exchanger with three-way catalyst (TWC) coated walls [11]. Different metallic heat exchangers were prototyped on a laboratory-scale and maximum conversion efficiencies of 84% were achieved [11]. Additional improvements implementing a standard ceramic monolith as the catalyst were found to increase overall conversion and performance under dynamic driving conditions when scaled to vehicle scales [11]. Rink et al. concludes that such systems can aide in the conversion of methane emissions of natural gas vehicles [11].

Hydrogen enrichment can potentially improve performance of natural gas engines through utilizing the fast burn speed of hydrogen to help mitigate some of the potentially negative effects of natural gas associated with natural gas combustion in an internal combustion engine, especially at lean burn conditions [12]–[14]. Ma et al. [12] examine the effect of using variable composition hydrogen/CNG mixtures (HCNG) on the thermal efficiency and emission of SI natural gas engines. The study found the introduction of HCNG extended the lean limit for natural as hydrogen percentage was increased in that the lean limit can be increased from an air-fuel equivalence ratio of 1.7 to an equivalence ratio of 2.4 for hydrogen percentages that increased from 0% to 50% [12]. Hydrogen enrichment was found to increase NO_x emissions and reduce thermal efficiency if engine spark timing was not

optimized [12]. For optimized spark timing, the thermal efficiency was found to increase while NO_x emissions were found to remain unchanged across all hydrogen concentrations [12]. For all situations, the unburned HC was found to always decrease with increased hydrogen concentrations, and thus the study concluded that with spark timing optimizations, hydrogen enrichment could be useful for reducing unburned HC without increasing NO_x emissions [12].

Mariana et al. [13] also experimented with various hydrogen and natural gas blends in SI engines. To study the engine performance under realistic operating conditions, a passenger car using a converted SI engine was tested over different drive cycles with various CNG and 15% and 30% hydrogen blends on a chassis dynamometer [13]. The study indicates that CO_2 emissions decreased with increasing hydrogen percentage and that fuel consumption was relatively unaffected for the lower hydrogen percentage and showed a moderate reduction for the higher hydrogen blend [13]. Natural gas combustion is shown to benefit from the addition of hydrogen due to the increased stability of hydrogen resulting in decreased combustion duration and cycle-to-cycle variability [12]–[14].

Zárante and Sodr  [14] evaluate the potential of operating SI engines on natural gas to reduce greenhouse gas emissions compared to the conventional operation on gasoline. A production four-cylinder engine was converted to run on natural gas using a commercial natural gas conversion kit and tested via a standardized emission test cycle to determine CO and CO_2 production under realistic vehicle operation [14]. The study resulted in greatly reduced CO emissions and reduced CO_2 emissions compared to gasoline such that all emissions were below current regulation levels even without a catalytic converter [14].

Homogeneous charge compression ignition (HCCI) engines are a current field of research in that they offer the ability to achieve high thermal efficiencies, and to significantly reduce harmful exhaust pollutants, specifically NO_x emission [15]. Kobayashi et al. [15] propose as turbocharged HCCI engine operating on natural gas as a relevant subject of investigation. Leaning out burn conditions for natural gas engines have proven to reduce NO_x emissions [7], [8], [15], and thus the ultra-lean burn conditions associated with HCCI operation lends itself as a potentially powerful technology to help reduce internal combustion engine emissions. Kobayashi et al. experimented with stationary turbocharged HCCI engines operating at various compression ratios and turbocharger boost pressures [15]. The results indicated that optimal thermal efficiencies and low NO_x emissions are achieved as the compression ratio is increased and the boost pressure is decreased [15] Kobayashi et al. concluded that an HCCI engine operating on natural gas offers great potential in combined heat and power generation, but not that additional research into additional engine control capabilities is necessary for practical use [15].

This work investigates the performance and emissions characteristics of a production six-cylinder, four-stroke outboard boat engine adapted to operate on natural gas using a conversion kit made available by Blue Gas Marine. Power and emissions readings were taken over a various range of engine speeds and engine loads. The motor was natural aspirated with port fuel injection and no after treatment of engine exhaust with devices that reduce pollutants such as a catalytic converter.

2 EXPERIMENT DESIGN AND SETUP

For this study, the sponsor desired to examine a popularly used, long-distance outboard motor for this study. A Yamaha F250 3.3L four-stroke outboard motor was chosen with manufacturer specifications as listed in Table 1 [16].

Table 1 - Engine Specifications

Engine Type	60° V6 DOHC 24-Valve
Displacement	204.6 ci (3352 cc)
Bore x Stroke	94 x 80.5 mm (3.70 x 3.17 in)
Prop Shaft Horsepower	250hp at 5500 rpm
Compression Ratio	9.9:1
Fuel/Induction System	EFI/VCT/DOHC
Exhaust	Through Propeller
Intake	Single Throttle Valve
Ignition System	TCI Micro Computer
Spark Plug	LFR6A-11-00-000
Alternator Output	44 Amp (Battery charge: 27 Amp)
Starting System	T = Electric w/ PTT
Lubrication	Wet Sump
Engine Oil Capacity	4.7L/4.5L w/without filter
Full Throttle RPM Range	5000 – 6000
Cooling	Water/Thermostatic Control
Recommended Engine Oil	Yamalube® 4M (See owner’s manual)
Recommended Fuel	Regular Unleaded (Minimum Pump Octane 89)
Recommended Fuel Filtration	Yamaha 10-Micron Fuel/Water Separating Filter
Ethanol Blend Limit	10% Maximum
Gear Ratio	(30:15) 2.00:1
Gear Shift	Forward, Neutral, Reverse
Shaft Length	X = 25”
Degree of Tilt	TBD
Degree of Trim	-3° through +16°
C.A.R.B. Rating	3-Star
Dry Weight	276 kg (608 lb)
Mounting Centers	28.6”
Steering Angle (maximum)	32° from center, either direction

The sponsor outfitted the stock Yamaha F250 with a natural gas conversion kit made available by Blue Gas Marine. The kit delivered natural gas to all six intake ports. For space optimization within the compact powerhead of the motor, the sponsor modified a set of commercially available single point gaseous injectors that individually delivered fuel to each intake port.

An engine test cell was developed in the laboratory equipped with engine-cooling, exhaust removal, and data collection systems. A water-brake dynamometer system was used to control engine speed and load, and a five-gas exhaust analyzer with a custom sampling probe was used to measure exhaust emissions. The following sections detail the experimental design and setup.

2.1 Dynamometer Set-up

A Land-and-Sea 13” toroid single-rotor water-brake absorber was used with Land-and-Sea DYNO-Max Pro software to measure and record engine speed and power output. The water-brake absorber loads the engine using resistance generated from the level of feed water supply in the absorber in order to control the resultant engine speed. A closed loop feed water system with a fixed supply water reservoir was used for absorber supply. A schematic of the feed water system is illustrated in Fig. 2. Supply water is pumped using the main supply pump to an engine control load valve. The load valve regulates the flow of water to the absorber depending upon the desired engine control conditions. The feed water then exits the absorber via the outlet and an auxiliary drain to a return basin. A return pump then returns the feed water collected in the return basin back to the supply reservoir. A secondary

reservoir-cooling pump draws water from the supply reservoir and cools it using a fan and radiator system in a secondary water loop.

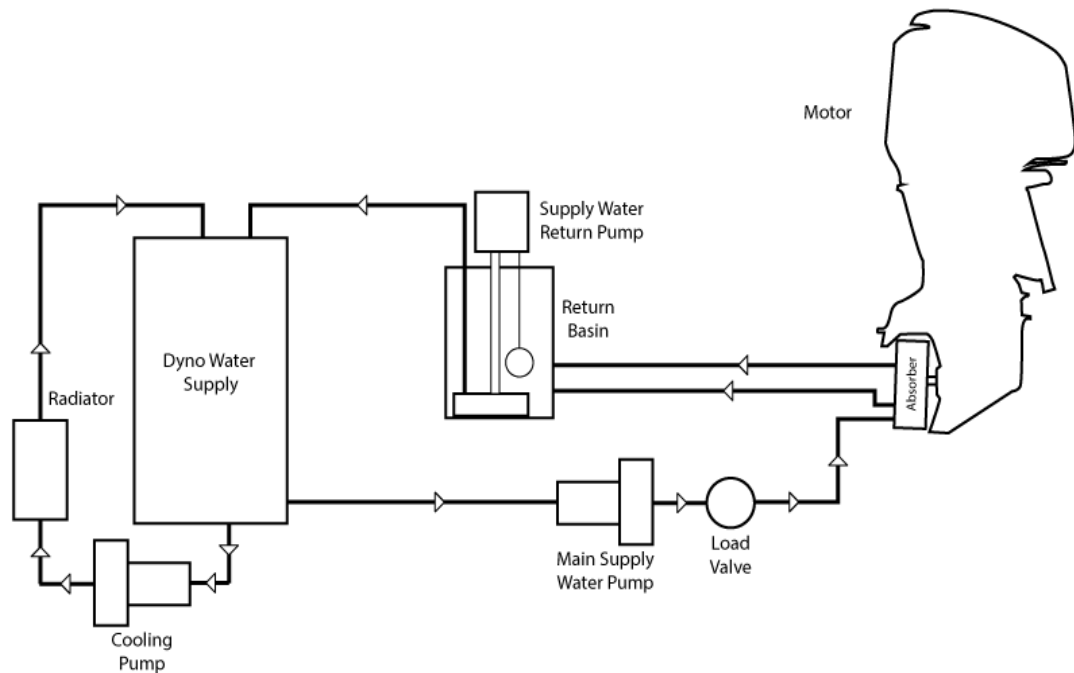


Figure 2 - Dynamometer feed water system

Adequate absorber and pump selection is critical for successful dynamometer operation. The sponsor chose the Land-and-Sea 13” water-brake absorber due to its maximum controllable engine power indicated at 400 hp, which would allow for the sufficient control of a 250 hp engine. The absorber is shown in Fig. 3. As seen in the figure, two large parts are included on the lower portion of the absorber and act as the inlet and outlets for the feed water. Also shown in the figure is a large torque arm with a strain gauge that is included on the absorber with universal stops that allow engine torque readings for

both clockwise and counter-clockwise engine outputs. The absorber utilizes an internal magnetic pickup to monitor the engine output shaft rotation speeds.

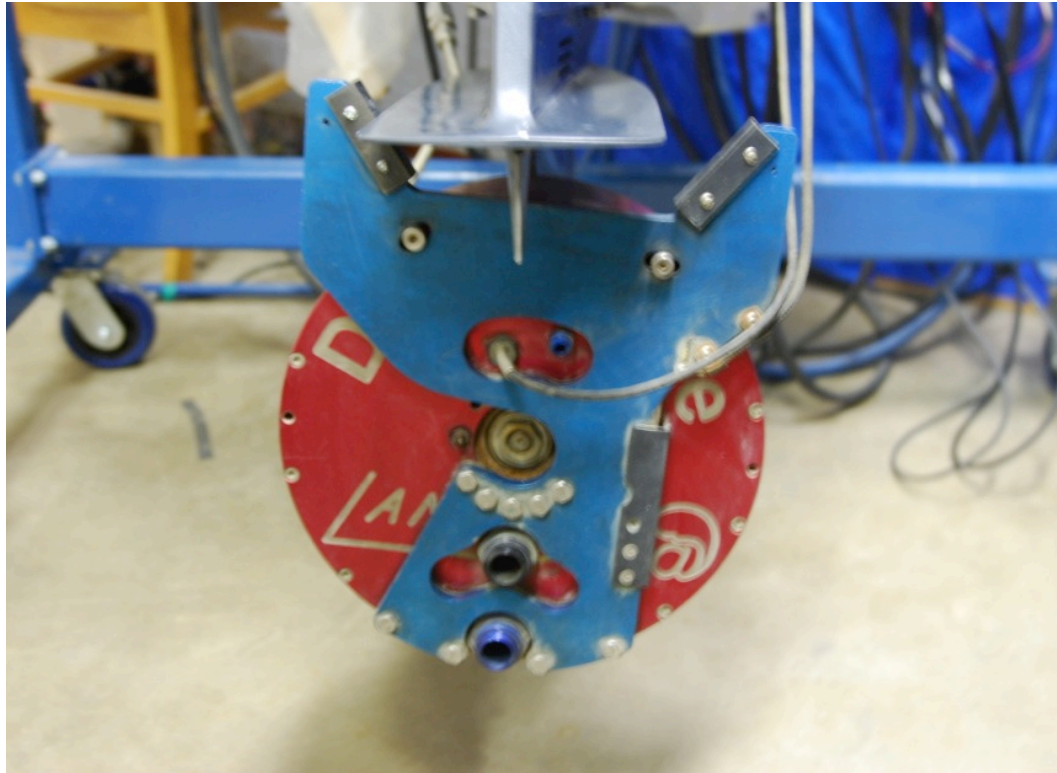


Figure 3 - Land-and-Sea water-brake absorber

The absorber mounts to the propeller shaft and, therefore, must be submersed in the cooling water tank. The marine version of the 13” toroid from Land-and-Sea is capable of being submerged in water and was chosen as the absorber for this study. The mounting configuration of the water-brake absorber on the propeller shaft is illustrated in Fig. 4.

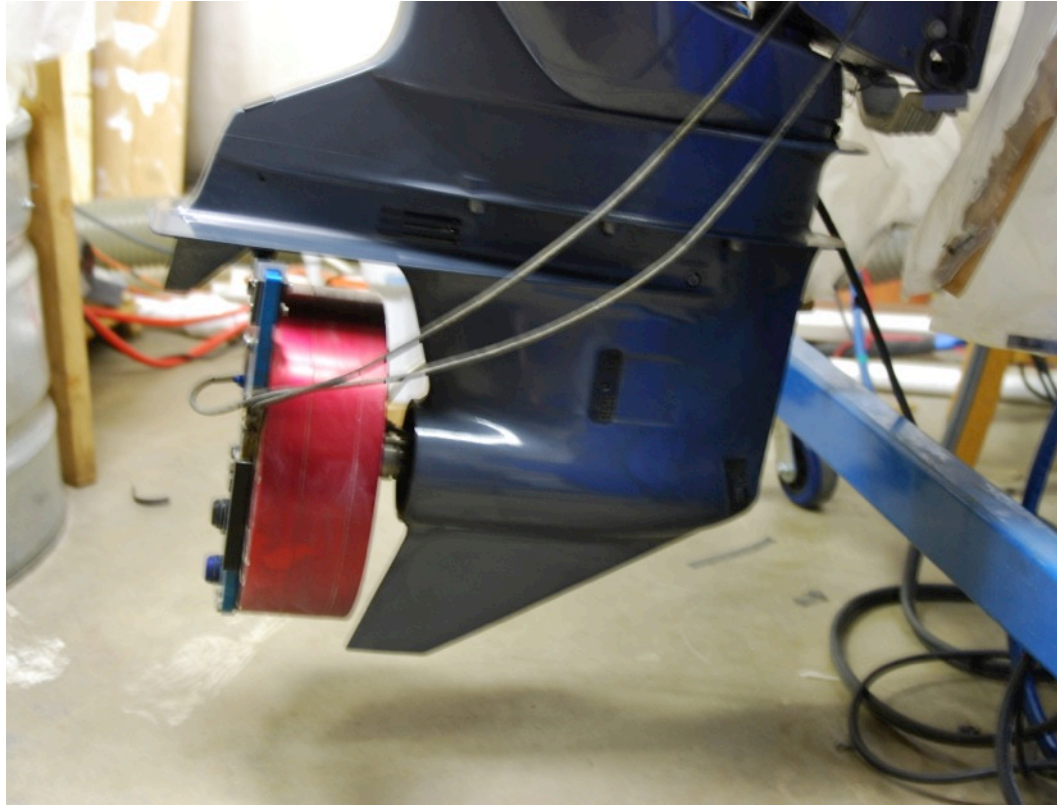


Figure 4 - Water-brake absorber mounting configuration

In order to achieve high loads, a sufficiently powerful pump is necessary to deliver high flows of water at the required pressures. According to [17], the supply pump must be able to deliver on the order of one gallon per minute of feed water to the absorber for every 20 horsepower at which the engine is rated. For the study's needs, a 250 hp motor would then require a total minimum flow rate of 12.5 gallons per minute to adequately control the engine. In order to overcome flow restrictions, [17] also specifies the minimum dynamic pressures needed at the previously indicated flow rates. A few of these values for various engine capabilities and the resulting determined requirement for the 250 hp motor are listed in Table 2. The indicated values were those supplied in the manufacturer's documentation

that were the closest the desired capability of the system to meet the rated maximum power of the test engine.

Table 2 - Dynamometer minimum feed water pump requirements

Power (hp)	Minimum Flow (gpm)	Minimum Pressure (psi)
200	10	18
250	12.5	21
400	20	30

Two main supply pumps were tested to determine their respective capabilities to adequately load the engine. The first was an Agri Supply Co. 1.5 hp pump with a 1.25" suction and 1" discharge. While the pump could adequately load the engine, the relatively small pump inlet and outlet tended to restrict flow and increase static to dynamic pressure drop, which made engine control in some situations sporadic. A Wayne 1.5 hp lawn sprinkler pump with a 2" suction and 1.5" discharge was then tried and was found to better satisfy the pump requirements with over 30 gallons per minute of flow and dynamic pressures within the specified range. The Wayne 1.5 hp lawn sprinkler pump is shown in Fig. 5. A small restrictor was placed in the outlet of the absorber in order to reduce the required flow for engine loading and decreased engine speed variation by slowing the rate of water loss from the absorber housing.



Figure 5 - Wayne 1.5 hp main feed water supply pump

For ease of testing and engine control, an automated electronic load valve was included in the dynamometer feed water supply system. The powered load valve was controlled via the DYNO-Max Pro software. An engine hold-RPM could be set and maintained automatically with the use of the electronic load valve while the engine operator could increase the engine throttle manually through an external remote control. The use of this load valve also enabled the use of automated power sweep tests in conjunction with the

DYNO-Max Pro software for measuring the wide-open engine performance over a swept engine speed range. The electronic load valve is shown in Fig. 6.



Figure 6 - Automated load control valve

The dynamometer feed water supply entering the absorber was constrained to remain below 180°F. For the closed-loop feed water system, this posed a potential issue in that as the absorber loaded the engine, the waste energy was transferred into the water within the absorber as heat and could potentially raise the water temperature above this threshold if the supply reservoir was not adequately sized and cooled. A 275-gallon high-density polyethylene intermediate bulk container (IBC) was used as a dynamometer water supply reservoir. The reservoir size was found to be sufficient for a full test cycle over a specified

engine speed. For extended testing, the secondary water-cooling loop with fan and radiator system was included to lessen reservoir-cooling time in between test runs. The radiator utilized in the cooling system was salvaged from a Ford Ranger, and a Wayne 1.0 hp sprinkler pump was used as the cooling loop auxiliary pump. The radiator and auxiliary pump are shown in Fig. 7.



Figure 7 - Fan and radiator system with reservoir cooling pump

2.2 Engine Cooling and Exhaust Removal

The use of an outboard motor proved to introduce a number of difficulties compared to traditional stand-alone engine test configurations. Due to the marine environment the

engine is designed to operate in, the engine cooling system does not use the traditional fan and radiator configuration that road vehicles typically utilize, but rather, the engine lower unit must be submersed in a body of water in which engine cooling water is gathered from rejected. Adequate cooling of the engine requires a substantial body of water with which the waste engine heat can be rejected without significantly raising the water temperature to temperatures that would cause the engine to overheat. For the engine size used with the experiment, a body of approximately 300 gallons was found to allow the engine to run well within the allowable engine temperature range for a period of at least an hour under any operating condition. A 300-gallon, galvanized water stock tank was used as an engine-cooling tank. The tank may be seen in Fig. 8.



Figure 8 - Engine-cooling tank and exhaust shroud

The marine application of this motor also introduced a difficulty around the safe capture and removal of engine exhaust from the test building. The motor does not have traditional exhaust pipes that could be easily ducted out of the building, but rather, the engine exhausts around the propeller into the transporting body of water. As the effective exhaust ports are submersed underwater, an alternative exhaust capture method was developed using an exhaust shroud and ventilation system. A wooden structure with large plastic sheeting was constructed around the engine-cooling water tank with an opening at one end for engine insertion and removal as seen in Fig. 8. Exhaust flow was removed from the shroud using a

large blower ventilating to the laboratory exterior with 6" diameter inlet tubing that was fed from a location at the rear of the exhaust shroud.



Figure 9 - Exhaust port location (left) and exhaust port close-up (right)

The location of the exhaust removal feed relative to the engine inlet location is illustrated on the left of Fig. 9, and a close-up view of this removal port is illustrated on the right of Fig. 9. The 6" diameter exhaust removal line is illustrated in Fig. 10 with the blower shown in Fig. 11.

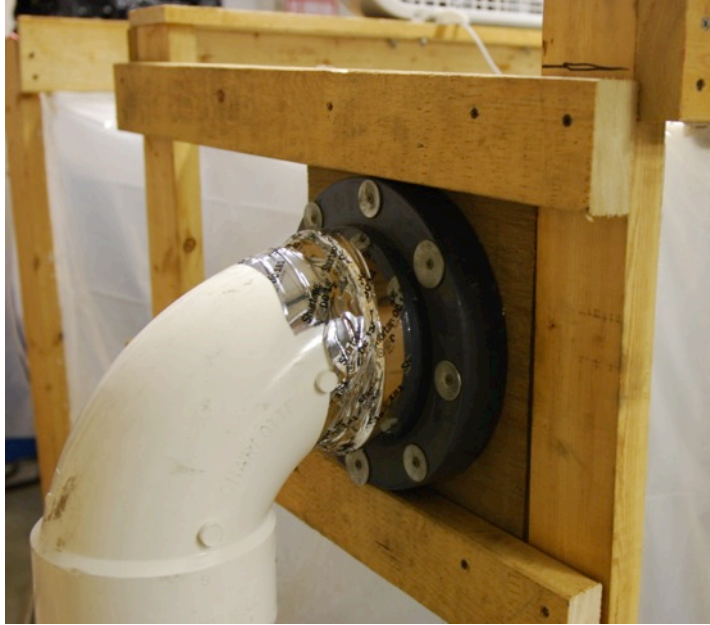


Figure 10 - Exhaust suction tubing



Figure 11 - Exhaust removal blower

Dynamometer feed water inlet, outlet, and drain lines were outfitted internally to the cooling water tank and exhaust shroud set-up to allow for proper water-brake absorber draining capabilities without compromising the effectiveness of the exhaust collection system. These internal delivery lines can be seen in Fig. 12, which illustrates the insertion point for the engine into the cooling and collection system.



Figure 12 - Engine cooling-tank insertion point with dynamometer absorber hook-ups

The shrouding system was continued onto the engine stand itself in order to allow for a rear seal at the point of engine insertion enabling a full enclosure of the exhaust shroud. The rear seal was secured to the left and right with screws to the wooden structure beams, and a magnetic tape strip was used for sealing along the lower seam. To aid with the removal

of exhaust from the shroud, the upper seam at the point of engine insertion was left unsealed to allow for an inflow of ambient air to direct exhaust flow when the blower suction was running. Additionally, two auxiliary zippers were introduced to the shroud near the engine insertion point in order to allow for a manual adjustment of total ambient inlet flow depending on the relative engine exhaust flow rate for a given engine speed. To help ensure the safety of the engine operator during testing, an Industrial Test Equipment, Inc. hazardous gas alarm was outfitted near the engine location and can be seen in Fig. 13.



Figure 13 - Hazardous gas alarm

Table 3 indicates the concentrations of the gases at which the hazardous gas alarm will activate.

Table 3 - Hazardous gas alarm thresholds

Gas	Alarm Threshold
Carbon Monoxide	150 ppm
Hydrogen	200 ppm
Methane	5000 ppm
Propane	420 ppm

2.3 Exhaust Measurement

CO, CO₂, excess O₂, NO_x, and unburned HC concentrations were measured using an Infrared Industries FGA4000XDS gas analyzer. The analyzer uses non-dispersive infrared (NDIR) technology to measure the CO, CO₂, and HC concentrations and an electrochemical cell to measure O₂ and NO_x concentrations [18]. The analyzer ranges for each measured gas are listed in Table 4 [18].

Table 4 - Exhaust gas analyzer measured gases and ranges

Gas	Range
Hydrocarbons (HC) (n-Hexane)	0 – 10,000 ppm
Carbon Monoxide (CO)	0 – 10%
Carbon Dioxide (CO ₂)	0 – 20%
Oxygen (O ₂)	0 – 25%
Oxides of Nitrogen (NO _x)	1- 5000 ppm

The analyzer utilizes a continuous water separation method to report the concentrations on a dry volume basis. The analyzer was also used to report the air-fuel ratio for gasoline measurements. Due to the marine intent of the engine, the lack of a traditional exhaust pipe required additional design elements for exhaust sampling. In order to retrieve as high quality of an exhaust sample as possible, there was a need to sample the exhaust stream before the exhaust met the engine-cooling water to avoid contaminating the sample. It was therefore determined that the optimal sampling location was inside the lower unit of the engine and close to the engine exhaust manifold. A custom sample probe was constructed out of stainless steel tubing and bent to conform to the exhaust flow channel at the propeller

shaft. The sample probe is shown after removal from the engine in Fig. 14. The sample probe configuration when it is inserted into the exhaust stream is shown in Fig. 15.



Figure 14 - Custom sample probe

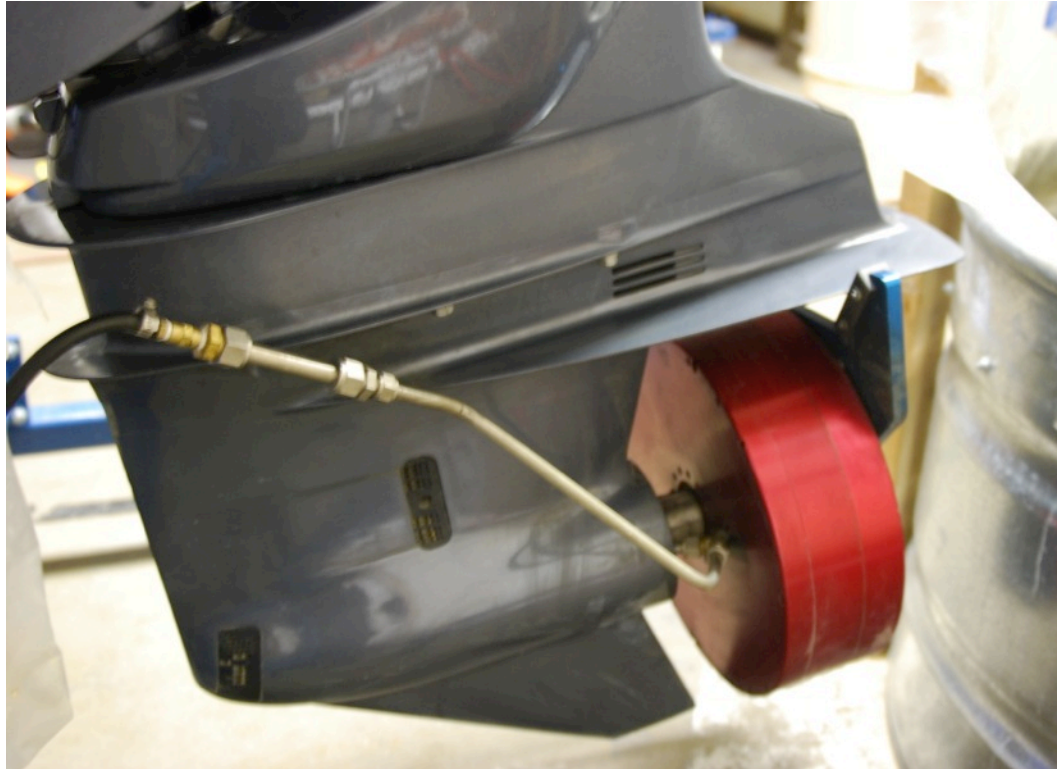


Figure 15 - Inserted sample probe configuration

2.4 Fuel Storage and Flow Measurement

The natural gas was stored as CNG. A type I steel cylinder was used as a fuel tank. The tank was considered full when filled to approximately 3000 psi. A system of high tubing and valves was constructed that enabled the cylinder to be refueled at a local CNG station or to allow natural gas to be delivered to a pressure reducer for delivery to the engine. After the reducer, flexible, flame-resistant hose was used to deliver the natural gas to the engine. An auxiliary valve with an open outlet allowed for natural gas remaining in the fuel line to be ventilated outside of the laboratory as needed at the conclusion of testing. A concrete, fenced

structure was constructed to house the CNG tank for public and laboratory safety. The CNG tank in the enclosure structure with feeds to the laboratory is shown in Fig. 16.



Figure 16 - CNG tank in enclosure

The high-pressure valve and tubing assembly is illustrated in Fig. 17. The main tank valve is located centrally and immediately at the tank port. A pressure gauge is included in the assembly for manual readings of the tank fill level when the tank valve is open. The tank refueling line is shown on the right. The use of this refueling line is controlled via the needle valve near the pressure gauge. When the needle valve to the left of the main tank valve is opened, natural gas is able to flow to a pressure reducer assembly for delivery to the engine

as needed. A pressure relief system is included after the needle valve to allow for automatic blow-off in the case of pressures surpassing 4000 psi.



Figure 17 - CNG tank refueling and delivery high-pressure valve and tubing configuration

Natural gas delivery to the engine was regulated using a pressure reducer and electro-valve configuration that was controlled via the natural gas control module (ECM) from the engine conversion kit. The natural gas pressure reducer system is shown in Fig. 18. The natural gas ECM could control flow into the reducer via a solenoid valve as seen in the

figure. The outlet natural gas pressure could be manually controlled using a setscrew on the reducer body. The natural gas ECM continuously monitored a pressure gauge and temperature sensor that are internal to the pressure reducer to determine fuel tank supply and to monitor the reducer temperature. Also seen in the figure, a secondary small diameter natural gas line used for the ECM pressure map that allows the system to monitor the absolute natural gas pressure delivered to the engine.



Figure 18 - CNG pressure reducer and electro-valve system

The natural gas was allowed to expand for pressure reduction and would freeze the pressure reducer components if not adequately warmed. The pressure reduction system was outfitted with warming lines in which water flowed from the engine-cooling tank through

internal channels in the reducer. The large body of water provided with the engine-cooling tank was more than sufficient for eliminating reducer freezing. A small water transfer pump was used to drive the reducer-heating loop during operation. This pump is shown in Fig. 19.

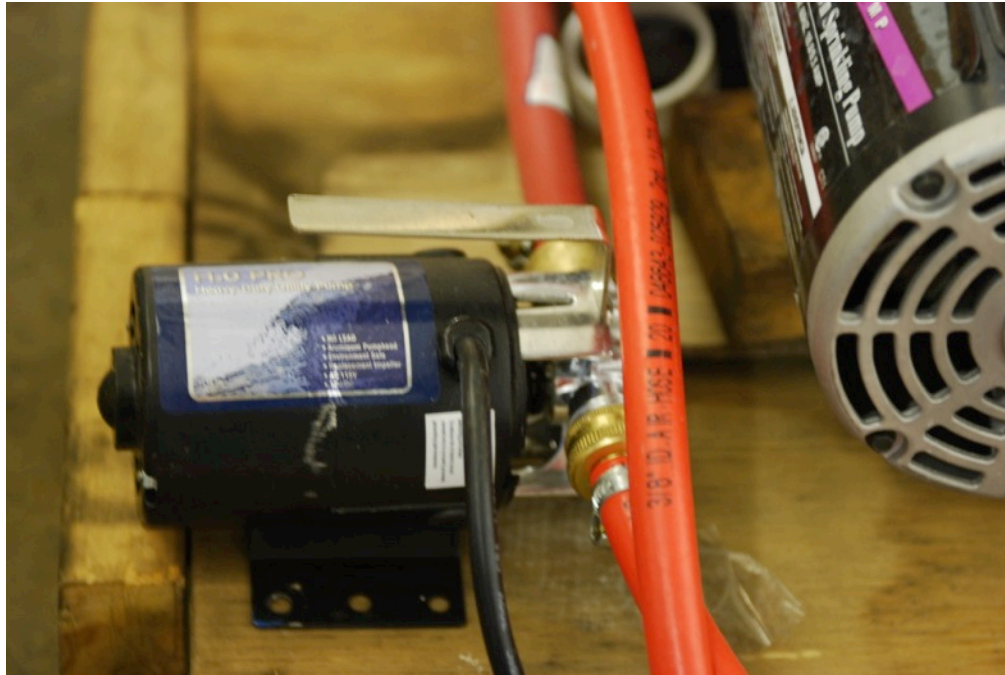


Figure 19 - Reducer warming water supply pump

The natural gas flow to the engine was measured using a gaseous mass flow meter. A Teledyne 200 series mass flow meter was used and is shown in Fig. 20. The mass flow range was reported for air at rates of 0-200 standard liters per minute. Corrections were used to account for the use of natural gas rather than air during testing.



Figure 20 - Teledyne series 200 mass flow meter

The gasoline was stored in a flammable liquid storage container in 5-gallon plastic gasoline storage tanks. For use in testing, a one-gallon tank was constructed for fuel flow measurements. The mass fuel flow rate of gasoline was measured using the one-gallon test tank and a digital scale. The test tank and scale configuration is shown in Fig. 21. A manual timer was used to determine the intervals for which a mass change took place to measure a mass flow rate.



Figure 21 - Gasoline tank and scale mass flow measurement configuration

2.5 Data Acquisition and Display

Fig. 22 illustrates the data acquisition set-up utilized for all aspects of the experiment. For engine control and performance measurements, a desktop computer running the DYNO-Max Pro software was used. A USB connection to a Land-and-Sea data computer and controller was to communicate between the computer and the various dynamometer components. The data computer is shown in Fig. 23. For power measurements, the engine speed pickup and load cell readings were transmitted to the data computer. The load valve

settings were also controlled and recorded to the data computer. Ambient temperature readings were recorded with a thermocouple linked to the data computer positioned near the engine operator. An external ambient absolute pressure gauge measured the pressure conditions within the laboratory.

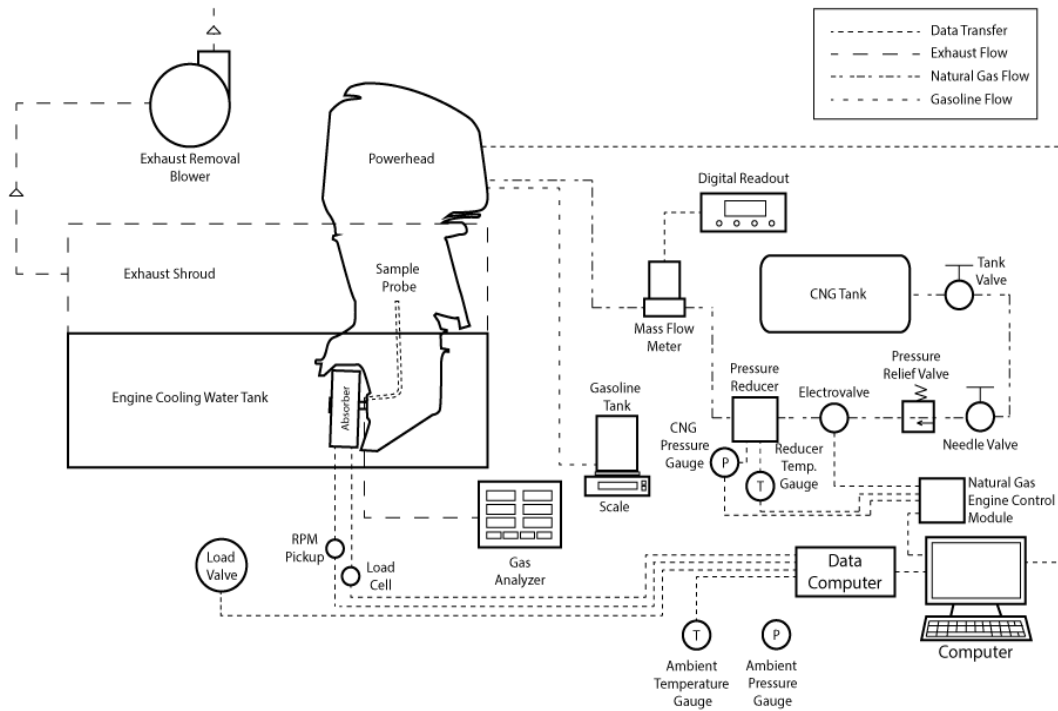


Figure 22 - Experimental data acquisition configuration



Figure 23 - Land-and-Sea data computer and controller

A second computer provided by sponsor could interface with the natural gas operating parameters using software included in the natural gas conversion kit. A USB connection allowed the software to take readings directly from the natural gas ECM. The ECM controlled the pressure reducer electro-valve, recorded the CNG pressure entering the reducer, recorded the reducer temperature, and recorded the map natural gas delivery temperature and pressure. The second computer could also interface with the original gasoline engine computer using Yamaha diagnostic software (Y-DIS). A USB connection directly connected the gasoline computer to the desktop computer for use with the Y-DIS.

As discussed previously, gasoline mass flow measurements were conducted using a fuel tank and scale system, and natural gas mass flow measurements were determined using a mass flow meter. Gasoline mass flow measurement readouts were calculated based on a digital stopwatch interface and the scale digital readout. The natural gas mass flow readings

were transmitted to a Hastings Instruments Model 40 power supply with digital display. The air-based mass flow measurements were read manually using the power supply digital display. The power supply is shown in Fig. 24.



Figure 24 - Mass flow meter power supply with digital display and exhaust gas analyzer

Exhaust measurements were read manually from the Infrared Industries FGA4000XDS five-gas analyzer. The analyzer contains six four-digit LED displays. The CO, CO₂, O₂, NO_x, HC, and air-fuel ratio values were displayed at all times across the six displays. A “hold” feature was included on the analyzer that could display a constant value

for each reading for data recording purposes. The analyzer and the displays as used in the experiment are shown in Fig. 24.

Each software component included its own customized display for data presentation. The DYNO-Max Pro software console display is shown in Fig. 25 on the right. The natural gas software display was monitored on the sponsor's secondary laptop computer in on the. At times the Y-DIS software was also used on the sponsor's computer to monitor engine diagnostic readings. Data from tests using the DYNO-Max Pro software could be exported in various file formats for external data analysis. All other readings were recorded manually into a laboratory notebook.



Figure 25 - Desktop computer with DYNO-Max Pro console display

3 RESULTS

3.1 Engine Performance

A water brake dynamometer system with an absorber with a magnetic speed pick-up and torque arm and strain gauge assembly was used to measure the engine output brake torque over swept engine speeds from 2500-5700 RPM for engine operation on both gasoline and natural gas. A fixed gear ratio of 2:1 is coupled between the engine crankshaft and the output shaft and is corrected for in the dynamometer software to output the correct relative brake torque and engine speed. The ambient temperature, absolute pressure, and relative humidity were also measured for each engine test, and the SAE air correction factors calculated from standardized reference tables were applied to the measured brake torque by [17]:

$$T_b = T_b^* C_p C_H C_T \quad (1)$$

where T_b^* is the measured brake torque, C_p is the absolute pressure correction factor, C_H is the relative humidity correction factor, and C_T is the temperature correction factor. Fig. 26 illustrates the air-corrected brake torque at the engine output shaft. It is clearly observed that the brake torque is significantly lower across all engine speeds for natural gas when compared to gasoline. The peak torque for gasoline was found to be close to 325 Nm, but the peak natural gas torque was found to be only 275 Nm, which corresponds to about a 15% reduction in maximum torque.

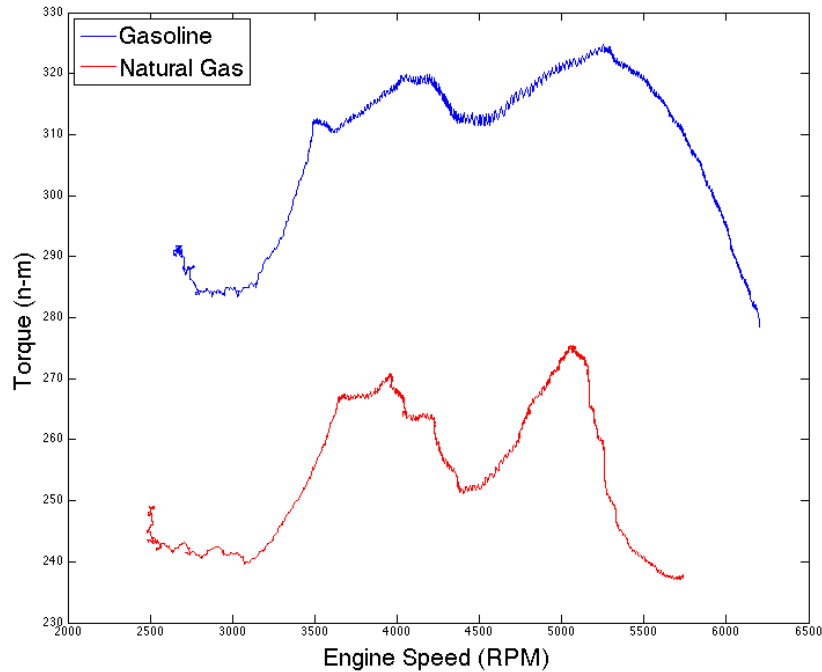


Figure 26 - SAE corrected brake torque for over swept engine speeds

The behavior of the torque curves over the specified engine speeds is interesting in that for both gasoline and natural gas the torque curves are generally bimodal. For both gasoline and natural gas, a peak is observed between 4000 and 4500 rpm and a second higher peak is observed between 5000 and 5500 rpm. For gasoline, the lower peak was observed to be 98.5% of the maximum gasoline peak torque, and the natural gas lower peak was observed to be 97.5% of the maximum natural gas peak torque. It is uncertain why there is a sudden drop in the torque curves for this engine, but after further investigation into other Yamaha outboard products, it was observed that the engine manufacturer produces two lower-rated power models of the same displacement engine [16]. Therefore, this torque drop

may have been intentionally designed into the engine control module map in order to produce a desired rated power output based on the engine manufacturer's market desires.

To further compare the performance of the engine operating on the test fuels, the brake engine power output was examined. The brake engine power, P_b , in kW is determined by [19]:

$$P_b = 2\pi NT_b \quad (2)$$

where N is the crankshaft rotational speed in revolutions per second and T_b is the brake torque at the absorber in Nm. The calculated brake power for the engine operating on the two test fuels is illustrated in Fig. 27. As with the torque, the gasoline power curve is consistently higher than the natural gas power curve. The gasoline peak engine power is observed to be close to 187 kW (about 251 hp) at around 5750 rpm, while the natural gas peak engine power is observed to be only about 147 kW (about 197 hp) at around 5100 rpm.

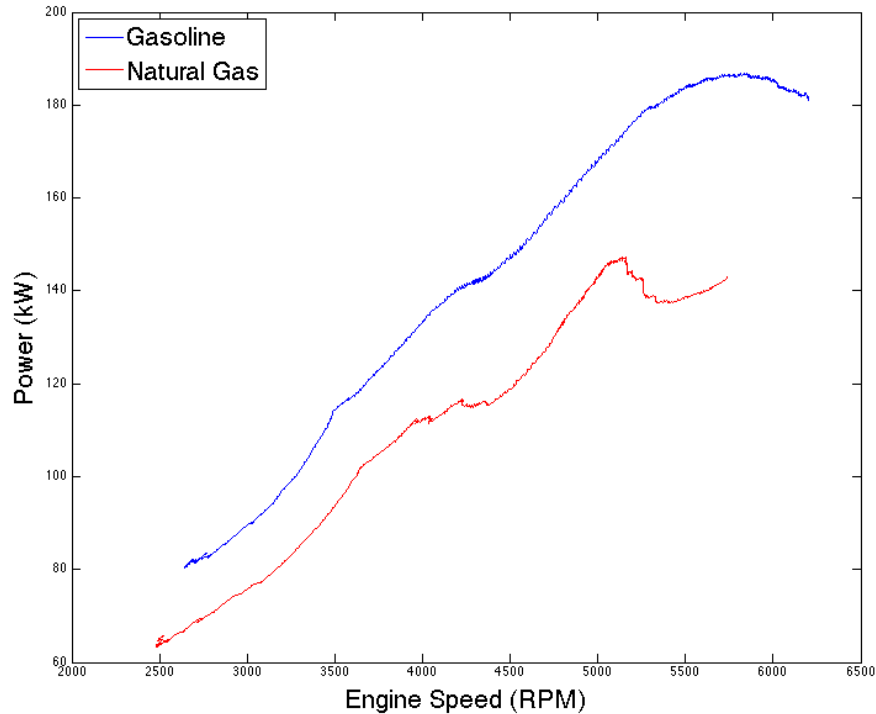


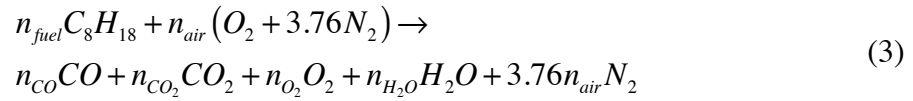
Figure 27 - SAE corrected brake power output over swept engine speeds

The reduction in rated horsepower was found to be near 21%. As seen from the previous power relation, achieving the same torque values at a lower engine speed will reduce power. While the peak torque decrease was determined to be near 15%, further examination and comparison of the torque curves show that the natural gas torque curve is slightly shifted towards lower engine speeds. This could, then, account for the larger decrease in peak brake engine power. This power decrease is thought to be in a large part due to volumetric efficiency losses due to the use of natural gas as a less dense gaseous fuel compared to gasoline [7]–[9]. The volumetric efficiency losses with natural gas limit the amount of fuel mass that can be taken into the cylinder for an equal air supply compared to gasoline. This is largely due to the relative densities of the fuel due to the different states of

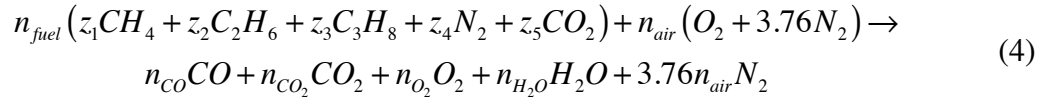
matter between fuels with the gaseous state of natural gas having injected densities around 2.5 kg/m³ and liquid gasoline having densities around 707 kg/m³ [20], [21, p. 701].

3.2 Major Exhaust Emissions

Non-stoichiometric combustion reactions were used to determine the inlet conditions to the cylinder based on exhaust gas measurements. For gasoline, the following general reaction was used to estimate the fuel and air conditions for each exhaust measurement:



where the n_i values correspond to the molar quantities of the indicated species. For natural gas, the following general reaction was used to estimate the fuel and air conditions for each exhaust measurement:



where the n_i values correspond to the molar quantities of the indicated species, and the z_i values correspond to the species fraction of the natural gas composition. Table 5 indicates the assumed natural gas compositions used in determining the combustion reactions [22].

Table 5 - Assumed natural gas composition

Species	i	z_i
Methane (CH ₄)	1	0.958
Ethane (C ₂ H ₆)	2	0.0290
Propane (C ₃ H ₈)	3	0.00400
Nitrogen (N ₂)	4	0.00800
Carbon Dioxide (CO ₂)	5	0.001

The major exhaust gas values were measured using the exhaust gas analyzer on a dry-basis as volume percentages. These recorded values were assumed as the molar quantities n_{CO} , n_{CO_2} , and n_{O_2} in the combustion products to determine the remaining molar quantities using species balance methods. The air-fuel ratio was measured using the exhaust gas analyzer for gasoline, but was calculated for natural gas due to the analyzer's programming. The natural gas air-fuel ratio was found using the following relation [21]:

$$A / F = \frac{m_{air}}{m_{fuel}} = \frac{M_{air} n_{air}}{M_{fuel} n_{fuel}} \quad (5)$$

where m_{air} is the mass of air, m_{fuel} is the mass of the fuel, M_{air} is the molar mass of air, and M_{fuel} is the molar mass of the fuel. In order to generalize the engine operation for comparison, the air-fuel equivalence ratio, λ , indicates the mixture composition relative to the stoichiometric conditions for a specific fuel. The air-fuel equivalence ratio for both gasoline and natural gas was generally determined by [19]:

$$\lambda = \frac{(A / F)}{(A / F)_s} \quad (6)$$

where $(A/F)_s$ indicates the stoichiometric air-fuel ratio. The measured exhaust gas compositions for CO, CO₂, and O₂ over the equivalence ratio range for gasoline are illustrated in Fig. 28. It is clearly seen that all three species concentrations are a strong function of the equivalence ratio. As the equivalence ratio increases from rich to stoichiometric conditions, the CO concentrations steadily decrease. A similar but opposite trend is observed for CO₂ concentrations in that these concentrations steadily increase with increasing equivalence ratios. O₂ concentrations remain level and small as the equivalence

ratio increases but begins to increase near stoichiometric conditions. The O_2 behavior is especially intuitive in that richer mixture compositions will consume all available O_2 for reaction assuming complete combustion, thus the O_2 concentrations would be assumed to be near zero for all rich mixtures and then steadily increase as the air-fuel mixture passes stoichiometric conditions and continues into increasingly lean conditions.

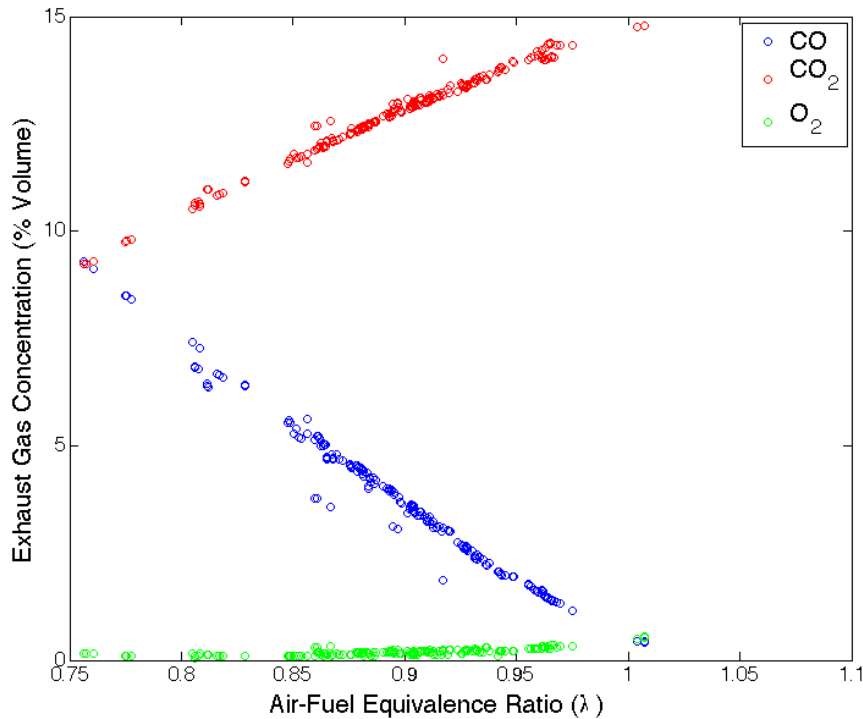


Figure 28 - Measured CO, CO₂, and O₂ concentrations for gasoline

Fig. 29 illustrates the measured exhaust gas compositions for CO, CO₂, and O₂ over the equivalence ratio range for natural gas. As opposed to gasoline, when operating on natural gas, the engine experienced a wide range of rich and lean conditions. Similar trends to gasoline for all three gases were observed for natural gas for rich conditions. As the

equivalence ratio increases past the stoichiometric point to lean conditions, the trends for all three gases change. After the stoichiometric point, CO₂ concentrations begin to decrease with increasing equivalence ratio. For CO, the steady decrease in concentrations observed for rich conditions quickly ceases and the CO concentration remains relatively constant and minimal for lean mixtures. Past the stoichiometric point, the O₂ concentrations rapidly increase with increasing lean conditions. For both gasoline and natural gas, these trends are consistent with those experienced in other research [7], [8], [19], [21].

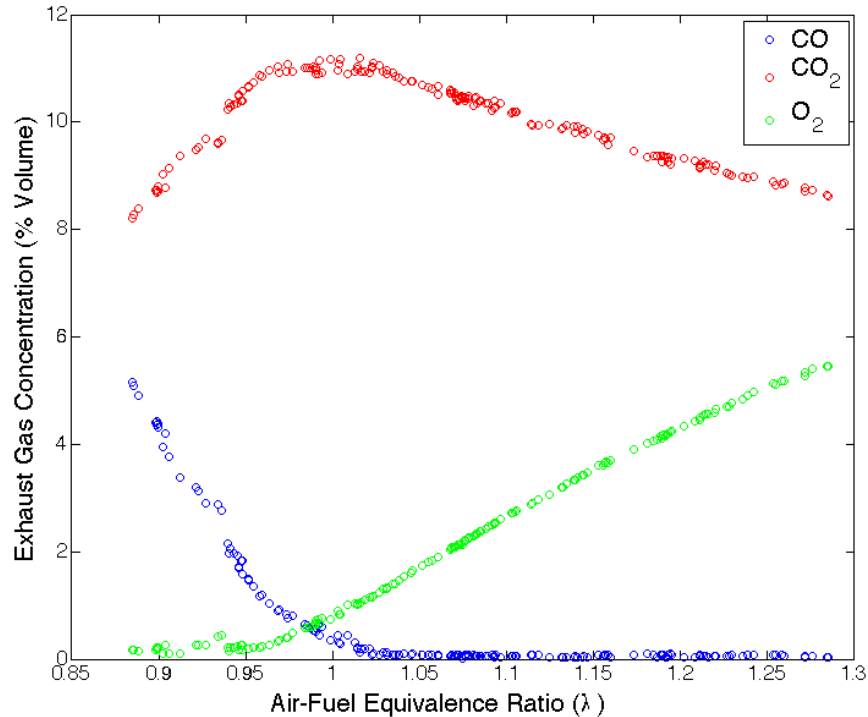


Figure 29 - Measured CO, CO₂, and O₂ concentrations for natural gas

To further compare the major exhaust gas components between the two fuels, the individual gas concentrations are compared to one another. Fig. 30 illustrates the comparison

of the CO concentrations between the two test fuels. As seen in the comparison, gasoline CO production is overall greater than natural gas with a peak gasoline concentration of 9.3% and a peak natural gas concentration of only 5.2%. However, when comparing the individual CO concentrations for the same air-fuel equivalence ratios, the produced CO concentrations were roughly equivalent with natural gas producing more CO for equivalence ratios between about 0.88 and 0.94, and gasoline producing more CO for equivalence ratios between about 0.94 and 1.

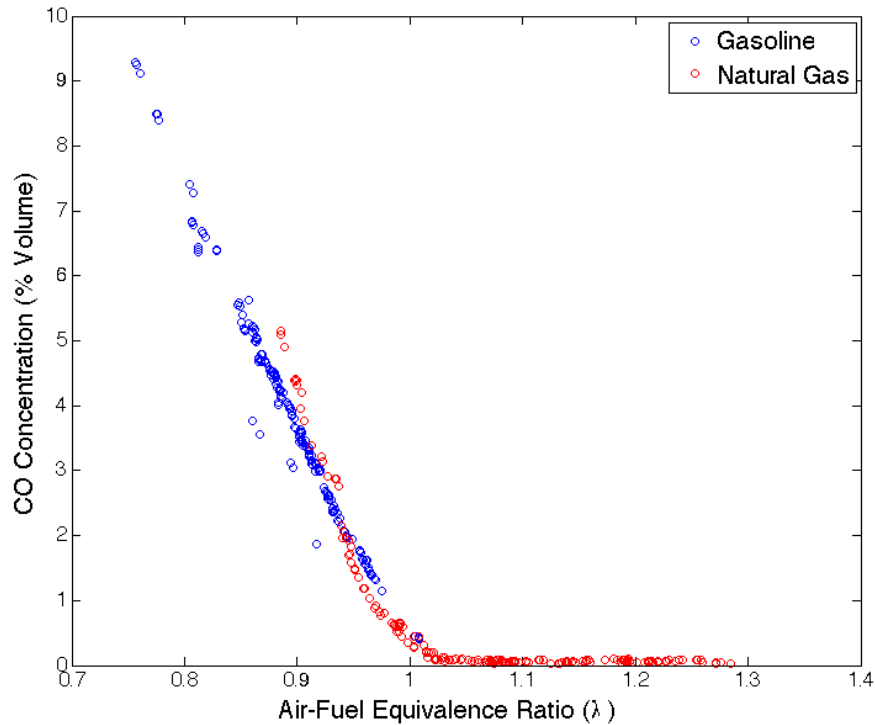


Figure 30 - CO comparison

Fig. 31 illustrates the comparison between CO₂ concentrations for the two test fuels. It is clearly observed that the gasoline CO₂ concentrations are considerably higher than those

of natural gas. The peak gasoline CO₂ concentration was measured to be close to 14.8% while the peak natural gas concentration was measured to be only 11.2%. For both fuels, this peak was observed near the stoichiometric point.

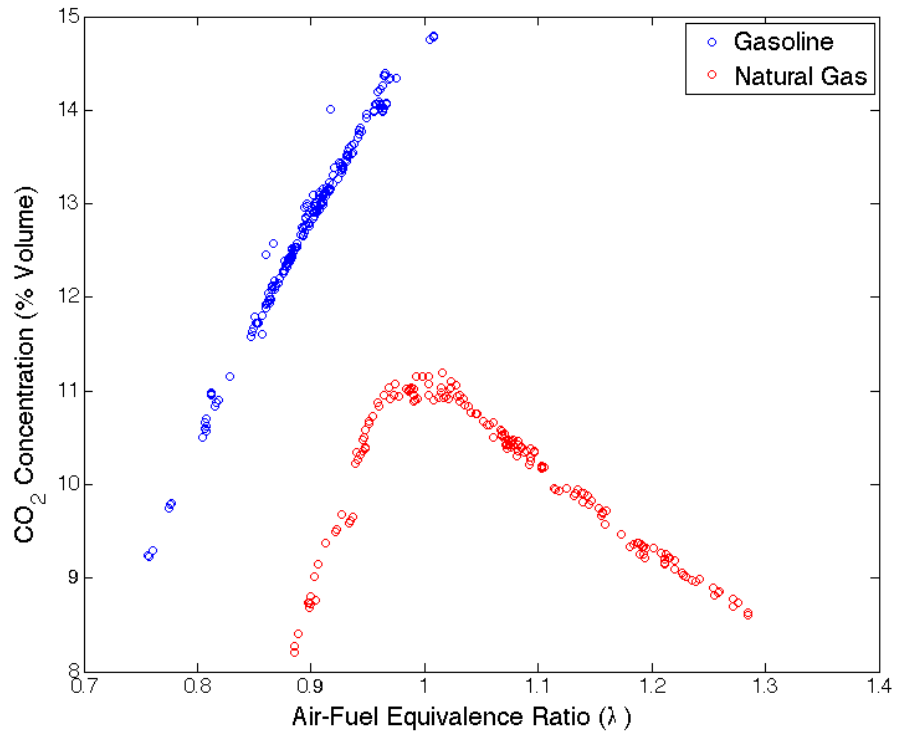


Figure 31 - CO₂ comparison

Fig. 32 illustrates the comparison of O₂ concentrations between gasoline and natural gas. For both fuels, the rich mixture O₂ concentrations are roughly equivalent and low in magnitude, which is expected for rich mixtures. Both the natural gas and gasoline O₂ concentrations begin to increase near the stoichiometric point at an equivalence ratio of about 0.95, and the natural gas concentrations rapidly increase as the operating conditions continue into the lean region.

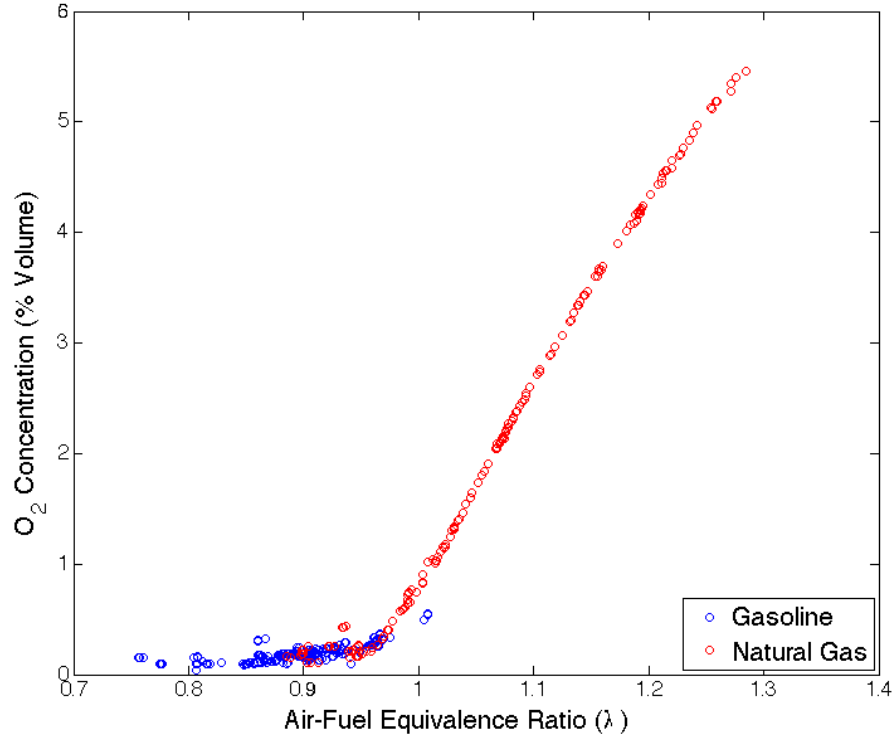


Figure 32 - O₂ comparison

3.3 Fuel Consumption, Fuel Conversion Efficiency, and Flame Temperature

Additional engine performance parameters to gauge the engine operation on the two test fuels were analyzed for comparison. While the engine torque provides a measure of the work potential, torque is largely dependent on engine displacement, and thus a parameter called the mean effective pressure is used to normalize the engine work over engine displacement [19]. The brake mean effective pressures was determined by [19]:

$$bmep = \frac{P_b n_R}{V_d N} \quad (7)$$

where n_R is the number of crank revolutions for each power stroke and V_d is the displacement volume. Similarly, the engine fuel consumption is related with the engine power output to

produce a useful comparison between different fuels called the specific fuel consumption.

The brake specific fuel consumption was found with [19]:

$$bsfc = \frac{\dot{m}_f}{P_b} \quad (8)$$

where \dot{m}_f is the mass flow rate per unit time. To provide a non-dimensional parameter as the measure of the engine efficiency, the specific fuel consumption is related with the heating value of the fuel. This fuel conversion efficiency is related to the bsfc by [19]:

$$n_f = \frac{1}{bsfc Q_{HV}} \quad (9)$$

where QHV is the heating value of the fuel. Table 6 indicates the heating values used for the determination of fuel conversion efficiency.

Table 6 - Assumed heating values

Fuel	Heating Value (Lower) (MJ/kg)
Gasoline [23]	43.448
Natural Gas [24]	49.060

A contour map of the specific fuel consumption for gasoline is illustrated in Fig. 33 over the measured engine speed range and bmep range. A best operating point is clearly observed near an engine speed of 4000 rpm and a bmep of around 950 kPa. This corresponds to a minimum bsfc value of around 238 g/kW-hr for gasoline. For the engine operating on gasoline at 4000 rpm, 950 kPa was achieved around 75-80% of maximum throttle. Gasoline specific fuel consumption increases as conditions move away from this optimum point with

the largest specific fuel consumption values occurring at the minimum bmep and low engine speeds.

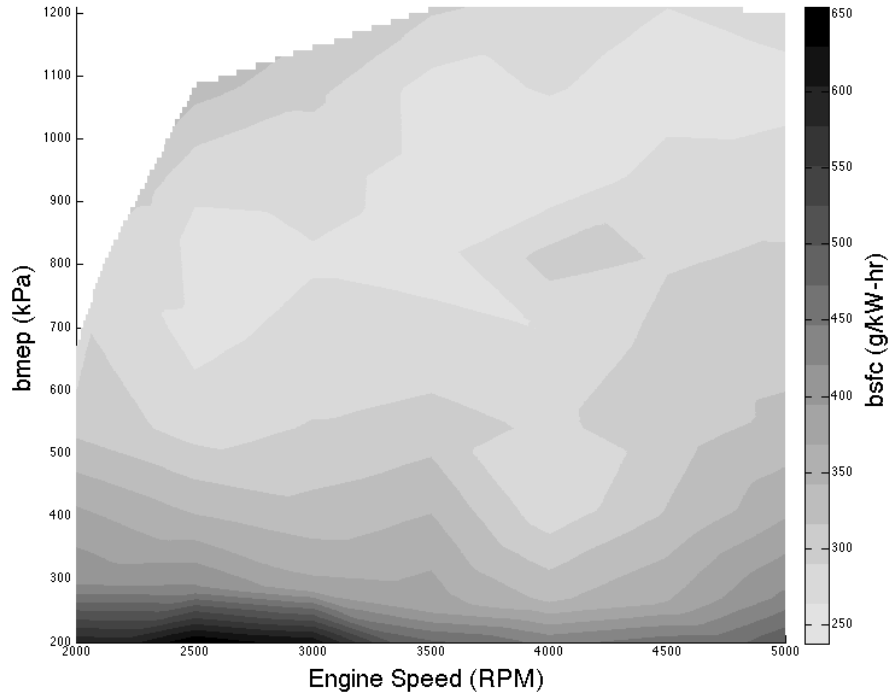


Figure 33 - Gasoline bsfc contour map

For natural gas, a contour map of the specific fuel consumption is shown in Fig. 34 over the measured engine speed range and bmep range for natural gas operation. The best operating point is less obvious when examining the contours for natural gas than for gasoline, but the lowest specific fuel consumption was observed around 5000 rpm and a bmep of around 1048 kPa. This corresponds to a minimum bsfc value of around 208 g/kW-hr for natural gas. For the engine operating on natural gas at 5000 rpm, 1048 kPa corresponds to the maximum throttle value. Natural gas specific fuel consumption increases as conditions move

away from this optimum point with the largest specific fuel consumption values occurring at the minimum bmep and low engine speeds.

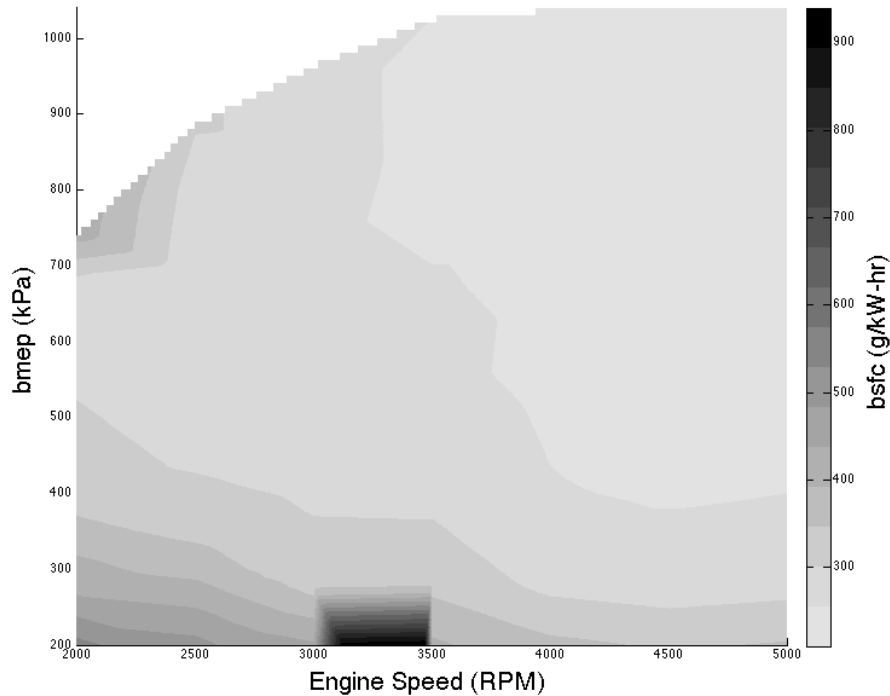


Figure 34 - Natural gas bsfc contour map

The specific fuel consumptions for the two test fuels are compared over the power outputs in Fig. 35. Both fuels share the same trend in that the bsfc values rapidly decrease initially with increasing power output, but then become relatively level for the remaining power output. While the comparison does not imply a large difference in specific fuel consumption between the two test fuels, natural gas did consistently achieve a reduction in specific fuel consumption on the order of 30 g/kW-hr across the power range. Between 30 and 60 kW, however, the lower range of the experienced gasoline bsfc values tended to

match those of natural gas, but as the power continued to increase, natural gas bsfc values tended to diverge from the gasoline values and gradually decrease until the natural gas power limit.

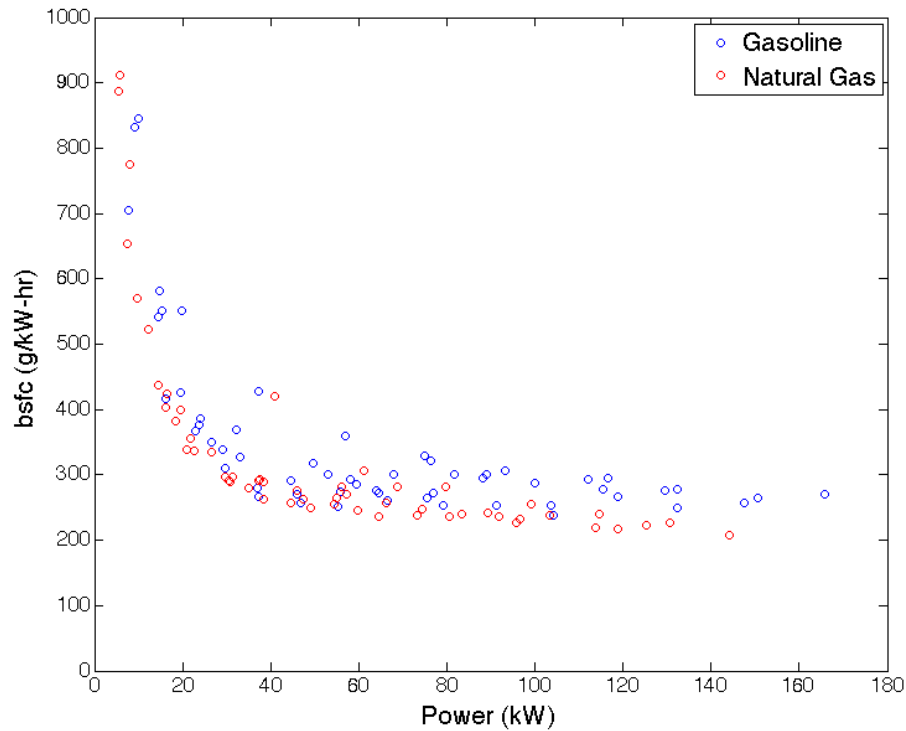


Figure 35 - Test fuel bsfc comparison

The fuel conversion efficiencies for the two test fuels were compared over the power output ranges as illustrated in Fig. 36. As with the bsfc comparison, the two fuels share the same general trend, however, the fuel efficiencies between the two fuels tend to be roughly more equivalent across the power out range rather than the general outperformance of natural gas to gasoline that was observed in the bsfc comparison. The upper range of gasoline fuel efficiencies between 30 and 100 kW actually tend to be higher than the upper range of

natural gas fuel efficiencies for the same power output. However, as the power range approaches the power limit, the natural gas operation tended to become slightly more fuel-efficient than gasoline on the order of 0.5%.

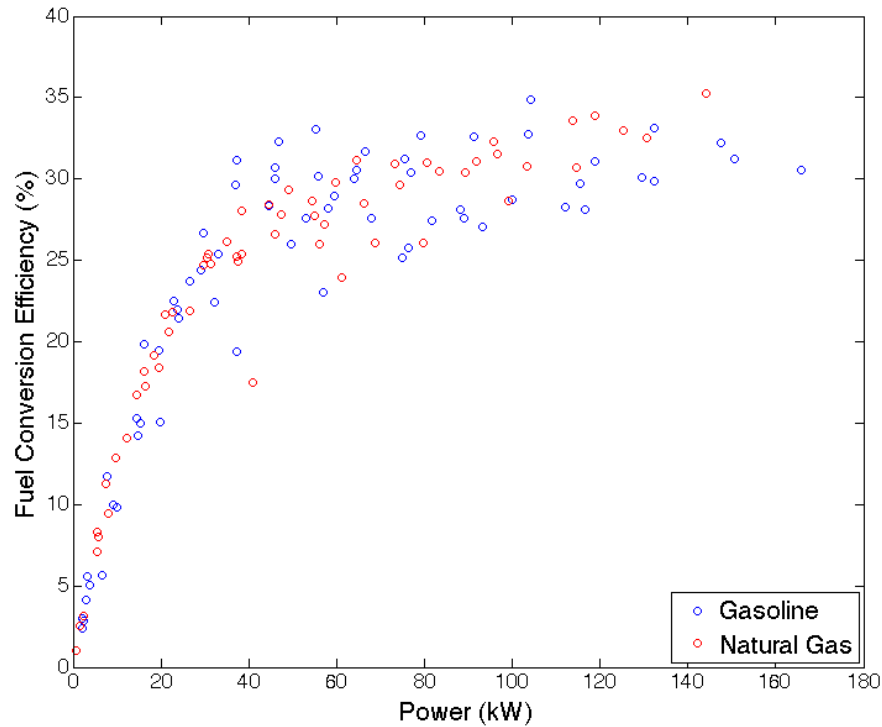


Figure 36 - Fuel conversion efficiency comparison

The adiabatic flame temperatures for the two fuels at each measured operating condition were determined by considering an energy balance between the products and reactants of combustion reactions assuming no heat losses were present. In reality, there is considerable heat transfer with the cylinder walls, and thus, the adiabatic flame temperature references the maximum attainable flame temperature the system could achieve. The general energy balance used is given as [21];

$$\Delta H = \sum_{\substack{j=1 \\ \text{prod.}}}^N n_j \left\{ (H_{T_f} - H_{T_0}) + (\Delta H_f^o)_{T_0} \right\}_j - \sum_{\substack{k=1 \\ \text{react.}}}^N n_k \left\{ (H_{T_i} - H_{T_0}) + (\Delta H_f^o)_{T_0} \right\}_k \quad (10)$$

where $(H_{T_f} - H_{T_0})$ indicates the enthalpy difference between the combustion product substance at the final reaction temperature compared to the reference temperature, $(H_{T_i} - H_{T_0})$ indicates the enthalpy difference between the combustion product substance at the initial reaction temperature compared to the reference temperature, and $(\Delta H_f^o)_{T_0}$ corresponds to the standard heat of formation of the substance.

The calculated adiabatic flame temperatures for both test fuels over the determined equivalence ratios are illustrated in Fig. 37. For both fuels, the adiabatic flame temperature was strongly governed by the equivalence ratio. The gasoline adiabatic flame temperature was found to be consistently higher than the natural gas adiabatic flame temperature for the same equivalence ratios. The peak adiabatic flame temperature of gasoline was found to be 2352 K while the peak natural gas adiabatic flame temperature was found to be only 2295 K. Due to the larger range of natural gas equivalence ratios, this peak is easily seen to occur around an equivalence ratio of about 0.95. Law et. al [25] examined this off-stoichiometric peaking of the adiabatic flame temperature to determine its cause. Their study concluded the rich shifting of the peak adiabatic flame temperature is primary due to factors associated with the maximum heat release, which was reduced by product dissociation. The study found that for hydrocarbon and air mixtures, there was greater dissociation on the lean mixture side, so

the peak adiabatic flame temperature tends to be shifted to the rich side of the equivalence ratio range.

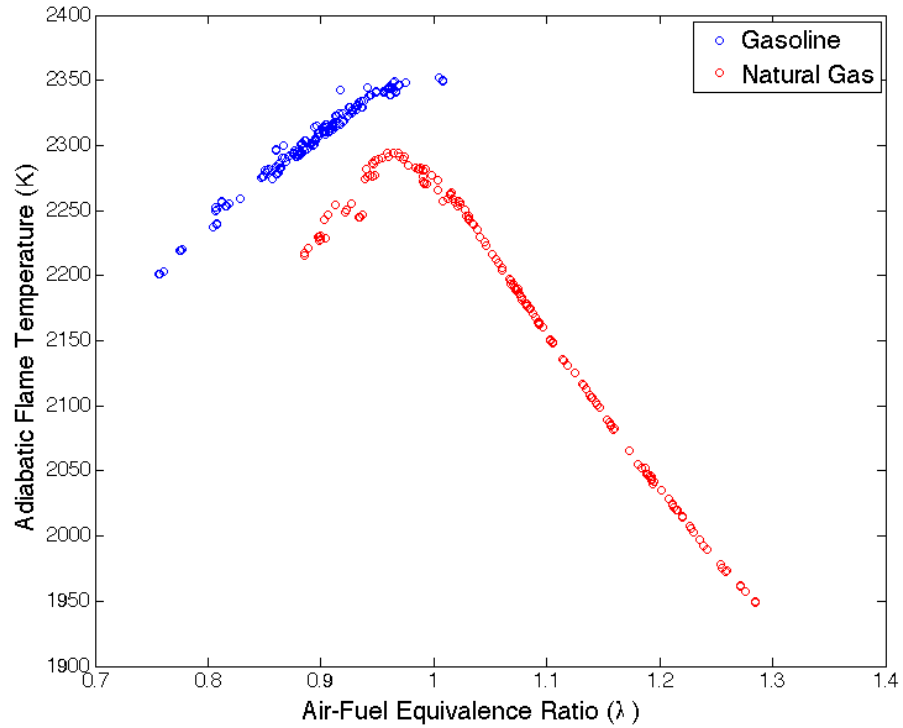


Figure 37 - Adiabatic flame temperature over equivalence ratio (K)

3.4 Pollutant Exhaust Emissions

The comparison between the productions of harmful exhaust emissions with respect to the two test fuels is particularly relevant in determining the quality of natural gas as an alternative to gasoline. Important substances for consideration are HC, CO, and NO_x emissions. In order to produce a more standardized measure of comparison in addition to the directly measured exhaust concentrations, the emission levels of each substance of interest is

normalized over the engine power output, is reported as specific emissions, and is determined by [19]:

$$sPart = \frac{\dot{m}_{part}}{P} \quad (11)$$

where \dot{m}_{part} indicates the mass flow rate of the substance of interest. These production rates of these harmful emissions were also normalized by the fuel flow rate to report the emission index given by [19]:

$$EI_{part} = \frac{\dot{m}_{part}}{\dot{m}_f} \quad (12)$$

where \dot{m}_{part} is reported in g/s and \dot{m}_f is reported in kg/s. To determine the mass flow rate of the NO_x emissions, the measured NO_x concentrations were assumed as entirely composed of NO.

Figures 38, 39, and 40 illustrate the interpolated contour maps for the specific HC, HC emissions index, and measured HC concentrations, respectively, for gasoline. All three parameters tend to show similar results for unburned hydrocarbon production for gasoline in that the minimal HC production for a given engine speed varies only marginally between the 200 to 800 kPa bmep range, but quickly increases outside of this range. One difference between the three parameters is that the sHC appears to have two peaks, one at full throttle near 3500 rpm and the other at low loads near 3000 rpm, while the emissions index and measured HC concentrations tend to not reflect the low load 3000 rpm peak. This could be due to the normalization by power in the sHC parameter in that the lower engine speed and low load conditions would do less to reduce the parameter value due to a low power output.

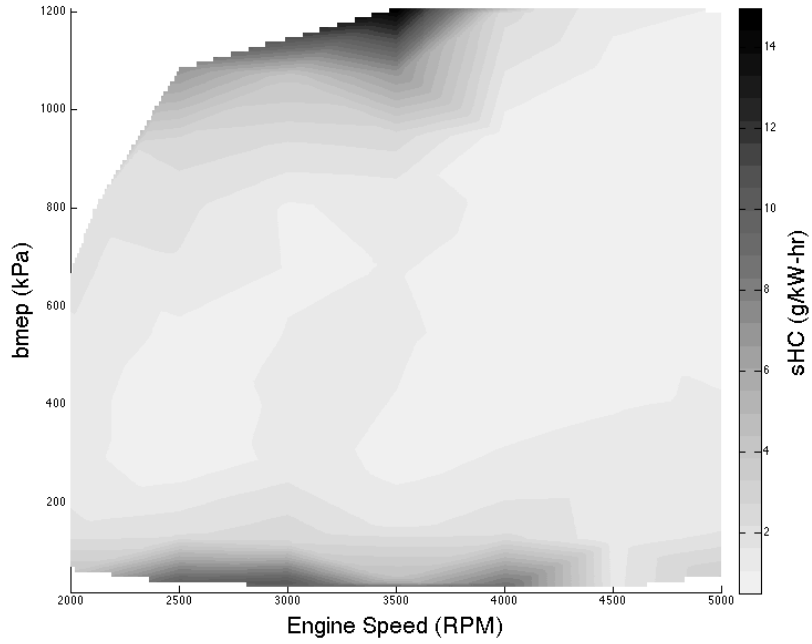


Figure 38 - Gasoline specific HC emissions contour map

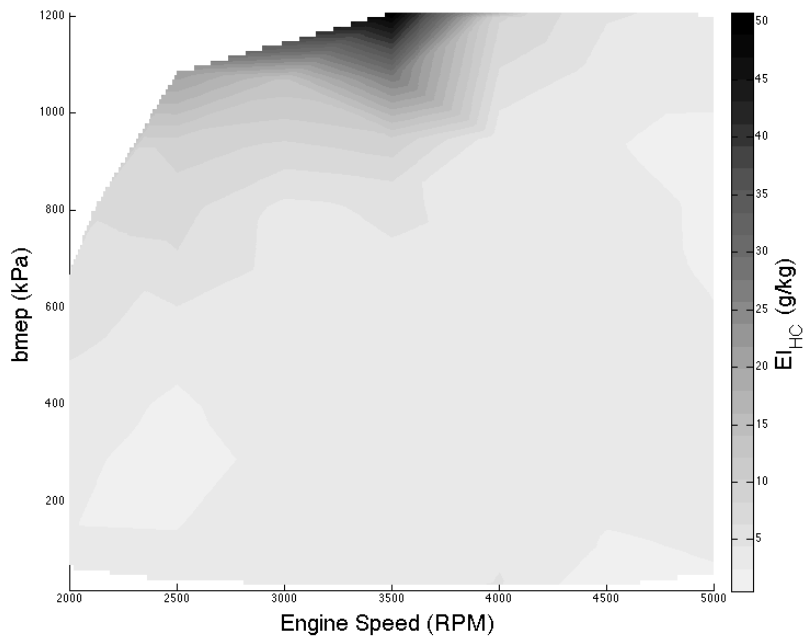


Figure 39 - Gasoline HC emissions index contour map

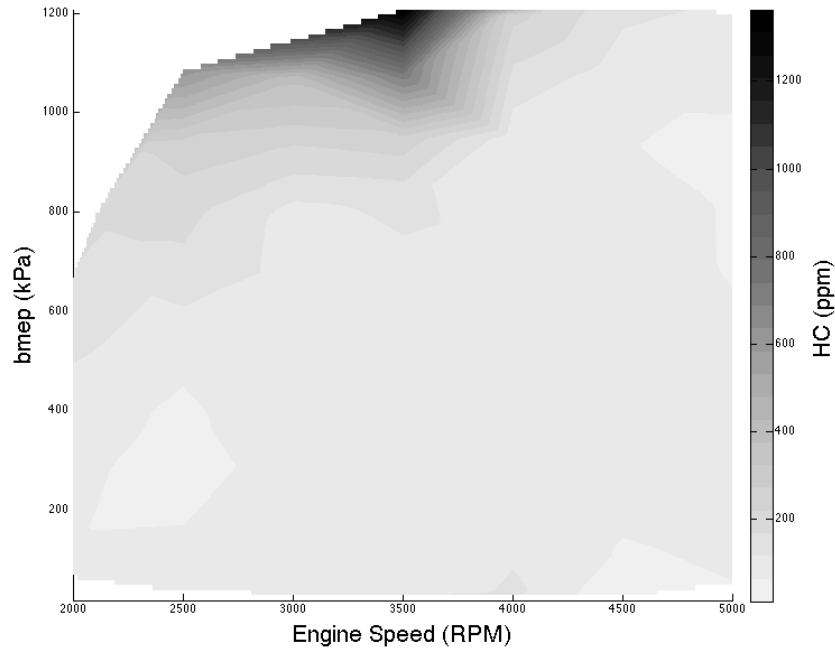


Figure 40 - Gasoline measured HC concentrations contour map

Figures 41, 42, and 43 illustrate the interpolated natural gas contour maps for the specific HC, HC emissions index, and measured HC concentrations, respectively. Again, all three parameters tend to show similar results for unburned hydrocarbon production for the test fuel. However, as opposed to gasoline, a localization of minimal HC production is recognized around the 4500 rpm and 600 to 800 kPa bmep range. As with gasoline, the greatest HC production parameters are reported at full throttle and 3500 rpm and at low engine speeds and engine loads. Conversely to gasoline, all three parameters tend to indicate the poor performance at low engine speed and engine load. Also, the sHC parameter for natural gas tends to not indicate substantially poor performance at 3500 rpm and full throttle. This indicates that for natural gas, the relative HC production at this point is small compared

to the power output even though this is the point of greatest HC production with respect to direct HC concentration measurements.

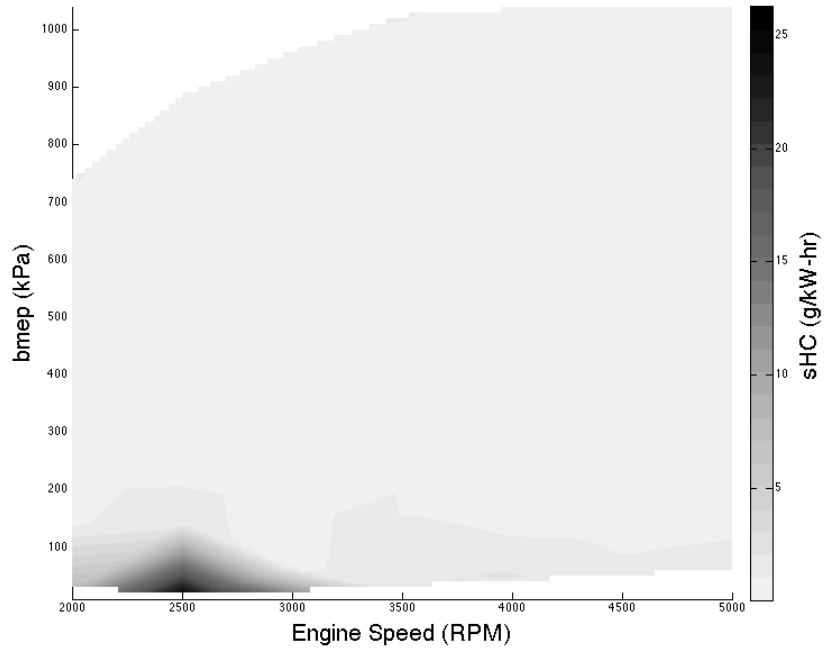


Figure 41 - Natural gas specific HC emissions contour map

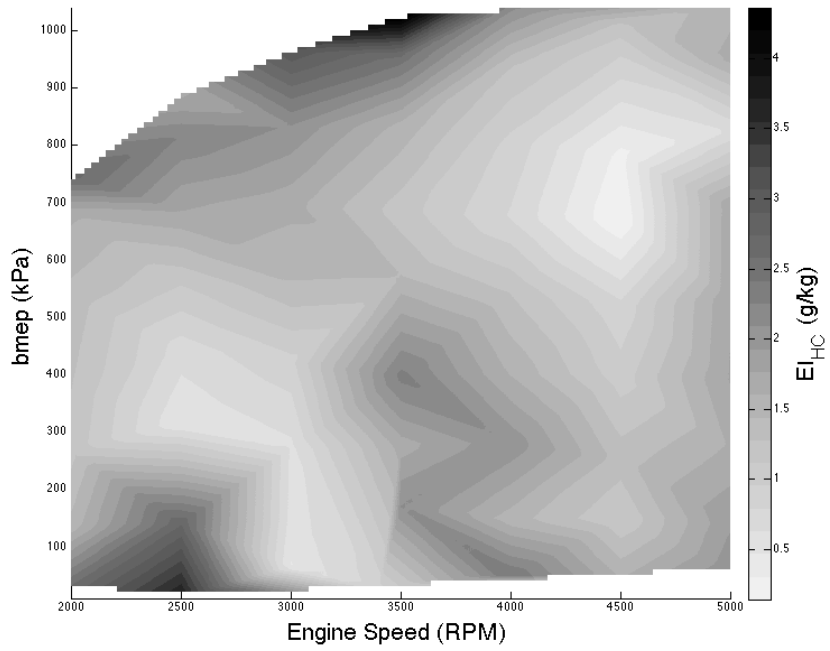


Figure 42 - Natural gas HC emissions index contour map

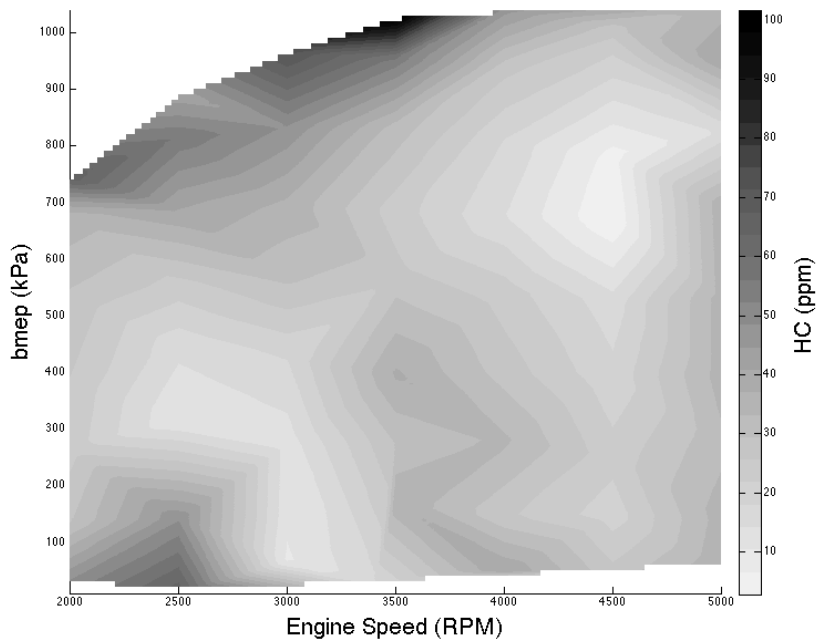


Figure 43 - Natural gas measured HC concentrations contour map

It is important to compare the relative scales of the three HC production parameters to recognize the overall performance of the two test fuels against each other. For specific unburned hydrocarbon production, the maximum determined sHC for gasoline was found to be about 15 g/kW-hr while the maximum sHC value for natural gas was determined to be about 36 g/kW-hr. Although the peak natural gas sHC value was greater than the peak gasoline value, natural gas was found to general produce less sHC emissions than gasoline for a majority of the data range. Between the 100 and 1000 kPa bmep range across all engine speeds, the natural gas sHC values were consistently determined to be below 1 g/kW-hr, but over the same range, the gasoline sHC values were only consistently below 3 g/kW-hr. The average specific HC emissions were, therefore, reduced by about 51% for natural gas engine operation. A similar trend is observed with the other two parameters except that the determined emissions index and measured HC concentrations were consistently lower than gasoline values across the entire range of measurement with a 71% reduction in the average HC emissions indexes and a 78% reduction in directly measured HC concentrations for natural gas against gasoline.

The specific production, emissions index, and directly measure concentrations of CO were then compared for gasoline and natural gas. Figures 44, 45, and 46 illustrate the interpolated contour plots of the three parameters for gasoline. Gasoline CO parameters experience similar trends to the gasoline HC parameters in that peak production occurs either at low loads or maximum throttle. The engine speed at which the highest CO production is recognized for full throttle is shifted from 3500 rpm for HC concentrations to around 3000 rpm. For engines speed of equal to or greater than 3500 rpm and above bmep values of 30

kPa, determined sCO values were less than about 2% of the maximum, CO emissions index values were less than about 18% of the maximum, and the directly measured CO concentrations were less than about 16% of the maximum measured values. Thus, it is evident that the greatest CO production conditions for the engine operating on gasoline were observed to be at low engine speeds and small loads.

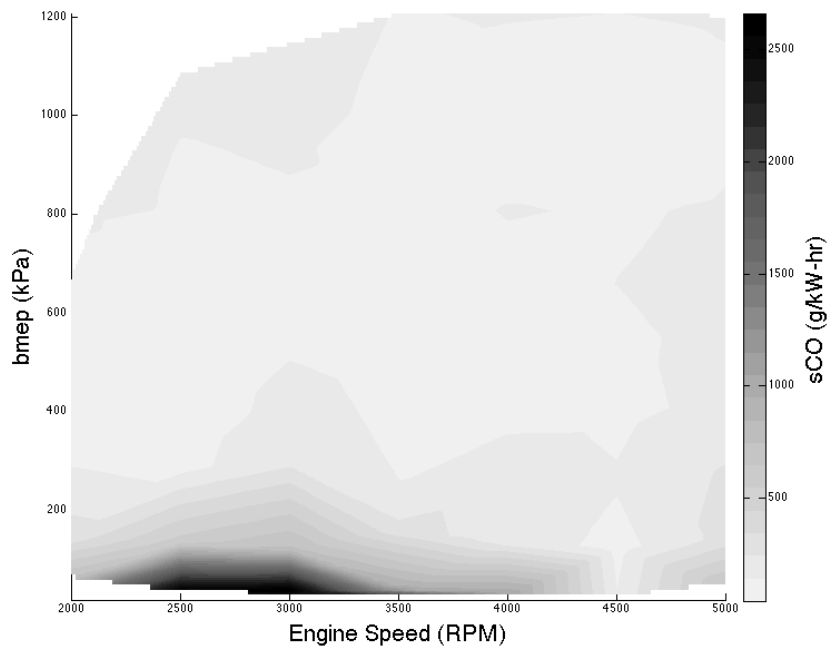


Figure 44 - Gasoline specific CO emissions contour map

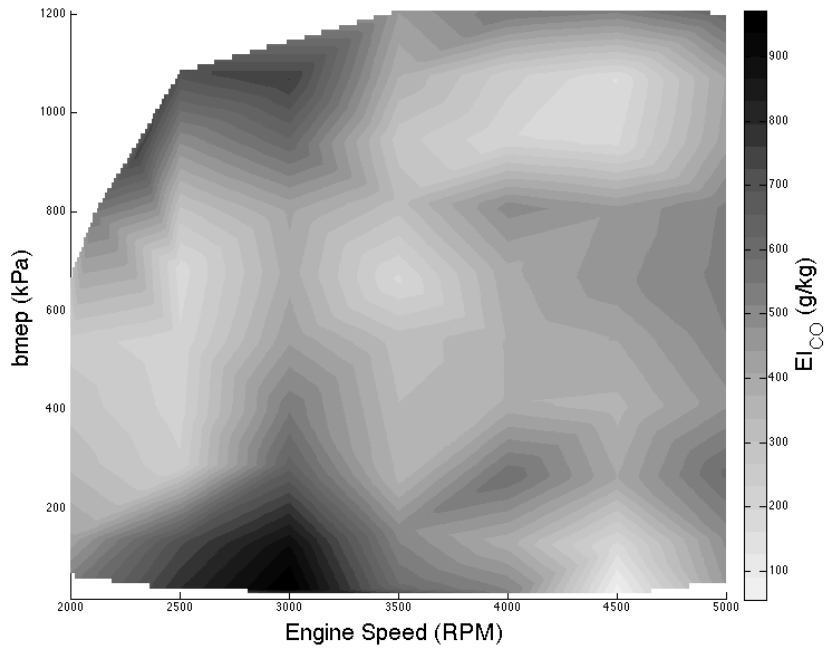


Figure 45 - Gasoline CO emissions index contour map

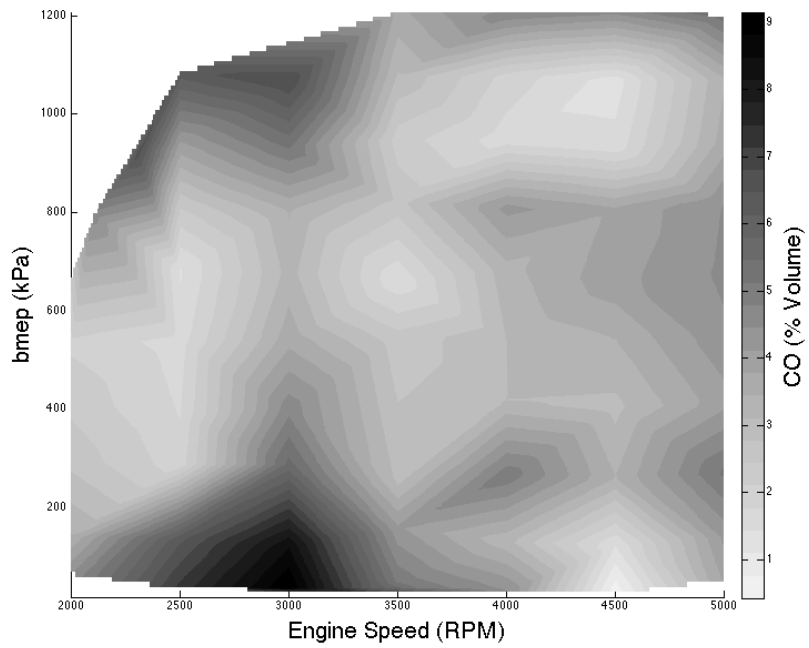


Figure 46 - Gasoline measured CO concentrations contour map

Figures 47, 48, and 49 illustrate the interpolated contour plots of the specific CO emissions, CO emissions index, and directly measured CO concentrations for natural gas. As with gasoline, the greatest CO production was observed near the maximum and minimum load conditions for a given engine speed. A localization of minimal CO production was observed for all three parameters between the engine speeds of 3000 to 4500 rpm and the bmep range of 250 to 850 kPa. For this range, the natural gas specific CO emissions and directly measured CO concentrations were less than 1% of the maximum respective determined values, and the CO emissions index was less than 2% of the maximum CO emissions index of the operating range. A local peak in specific CO emissions was observed at minimal engine speeds and minimal load conditions, which is not observed with the emissions index or measured gas concentrations. Another local peak was recognized for all three CO emissions parameters at the 5000 rpm engine speed. This peak occurs around a bmep value of 950 kPa, which corresponds to about 90% of full throttle.

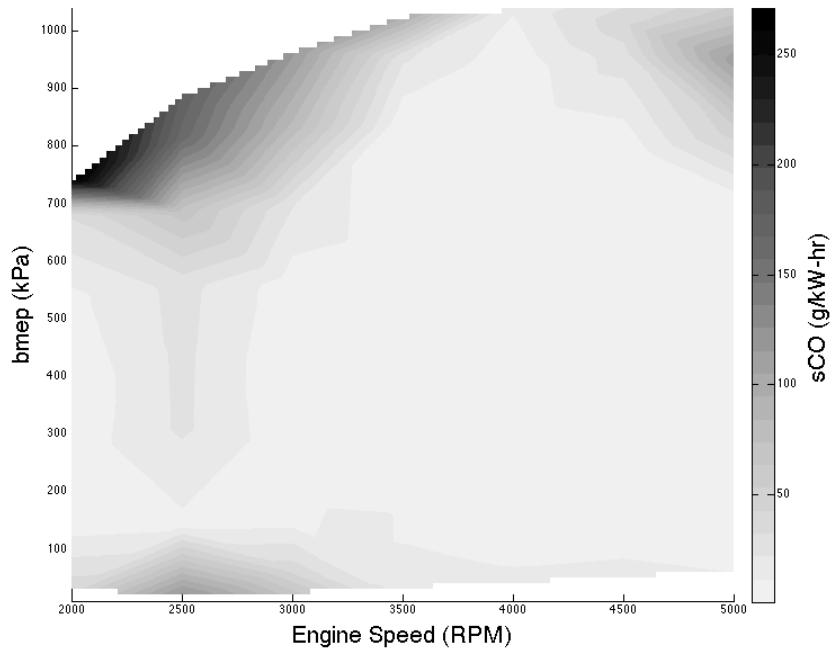


Figure 47 - Natural gas specific CO emissions contour map

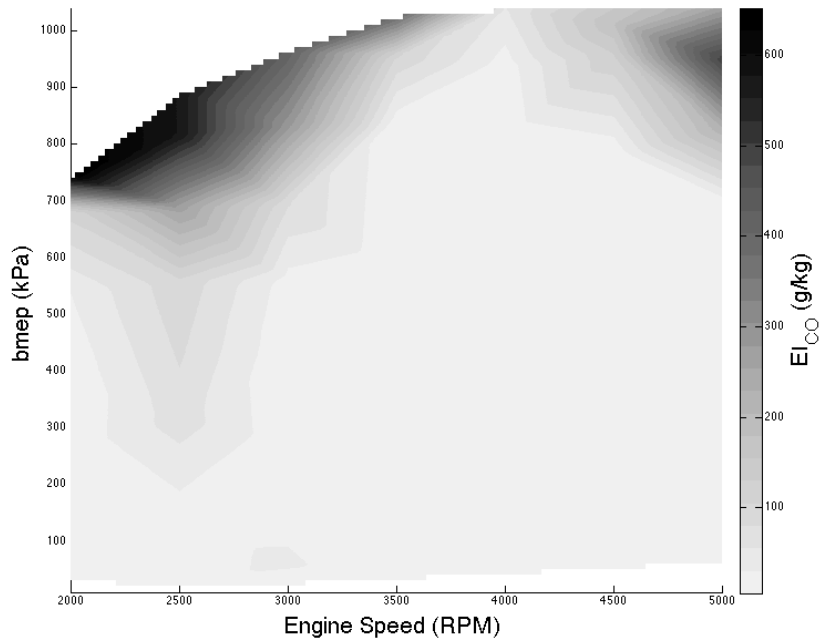


Figure 48 - Natural gas CO emissions index contour map

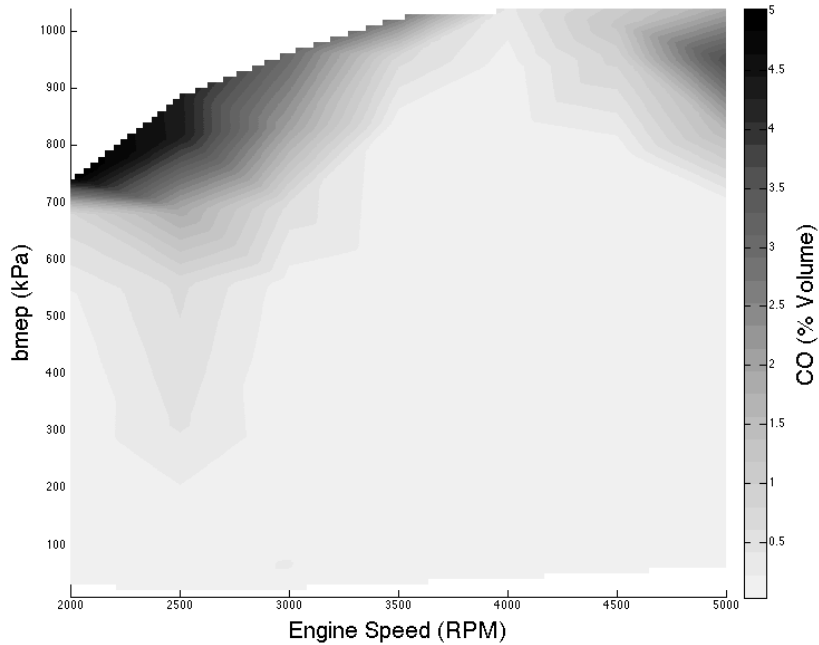


Figure 49 - Natural gas measured CO concentrations contour map

While the gasoline and natural gas CO emissions parameters tend to share similar aspects of trends, a comparison of the relative scales of these parameters between the fuels is necessary. A comparison of the specific CO emissions for gasoline and natural gas revealed a substantial decrease in specific CO emissions for natural gas engine operation against gasoline operation. The peak gasoline specific CO emissions value was determined as 2864 g/kW-hr, while the peak natural gas specific CO emissions value was only 280 g/kW-hr. This corresponds to a 90% reduction in specific CO emissions when operating on natural gas. The average gasoline specific emissions value across all operating conditions was found to be near 280 g/kW-hr, and the natural gas average specific CO emissions values was determined to be about 31 g/kW-hr. The average reduction in sCO values from gasoline to natural gas was, therefore, found to be about 89%, which is consistent with the reduction of the peak

values. When comparing the CO emissions indexes for gasoline and natural gas, the peak CO emissions indexes were reduced by approximately 32% from 938 g/kg to 668 g/kg for gasoline and natural gas respectively, while the average CO emissions indexes were reduced by about 78% from 442 g/kg to 94 g/kg. Similarly, the peak measured CO concentrations were reduced from 9.29% to 5.16% indicating a 44% reduction in peak CO concentrations, and the average measured CO concentrations were reduced from 3.78% to 0.67% indicating an 82% average reduction in CO concentrations with natural gas across all operating conditions.

To visualize the NO_x emissions parameters for gasoline, Figures 50, 51, and 52 illustrate the specific NO_x emissions, the NO_x emissions index, and the directly measured NO_x concentrations. The emissions index values and measured NO_x concentrations reflected similar results with a localized peak near an engine speed of 4000 rpm and mean effective pressure of 947 kPa. For the specific NO_x emissions, occurred as a local maximum, but for the entire operation range, the peak specific NO_x emissions were reported at low engine loads and the highest engine speeds. In general, NO_x emissions parameters increased with increasing engine speed until speeds of 4000-4500 rpm and then began to decrease at higher engine speeds. The NO_x emissions parameters also tended to increase with increasing mean effective pressures until 70-90% of full-throttle occurred and then began to decrease at maximum engine loads.

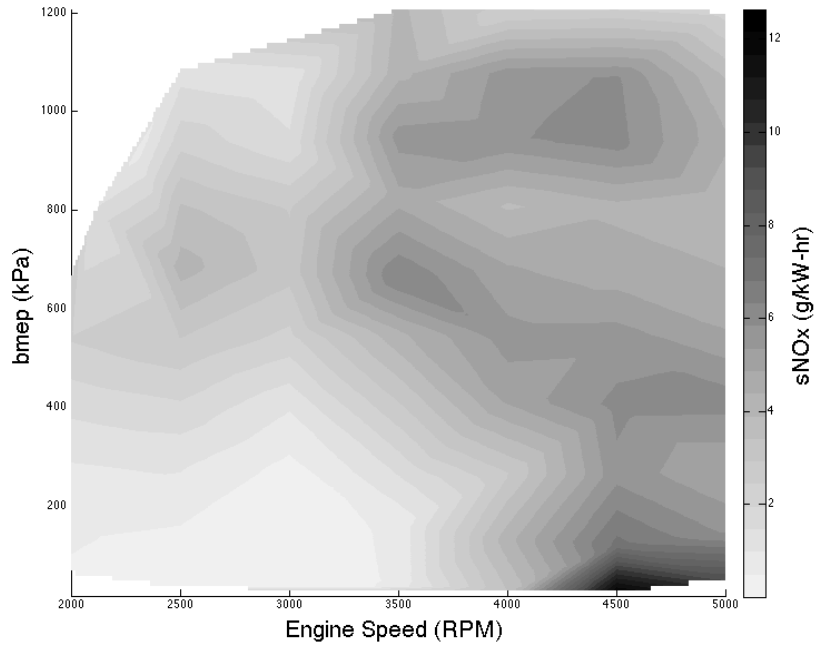


Figure 50 - Gasoline specific NO_x emissions contour map

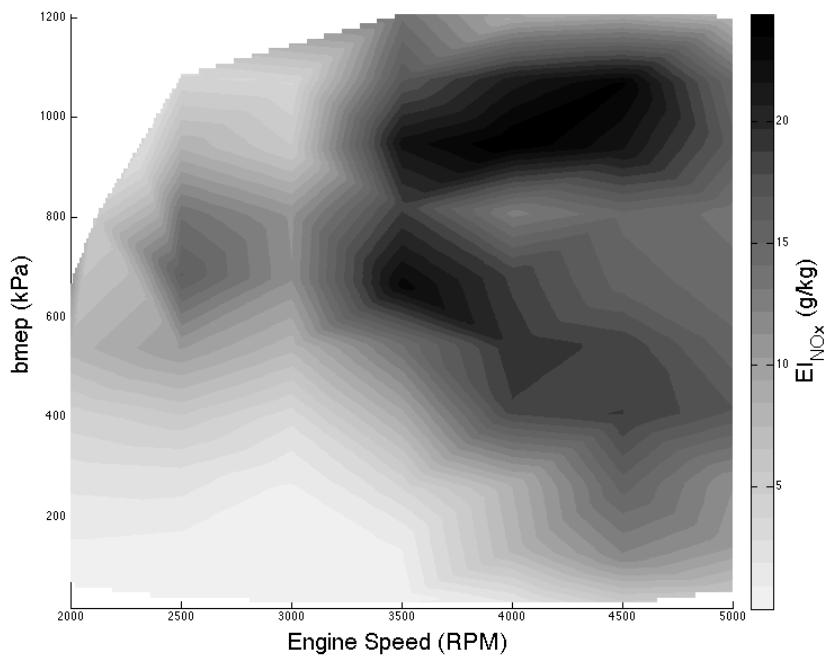


Figure 51 - Gasoline NO_x emissions index contour map

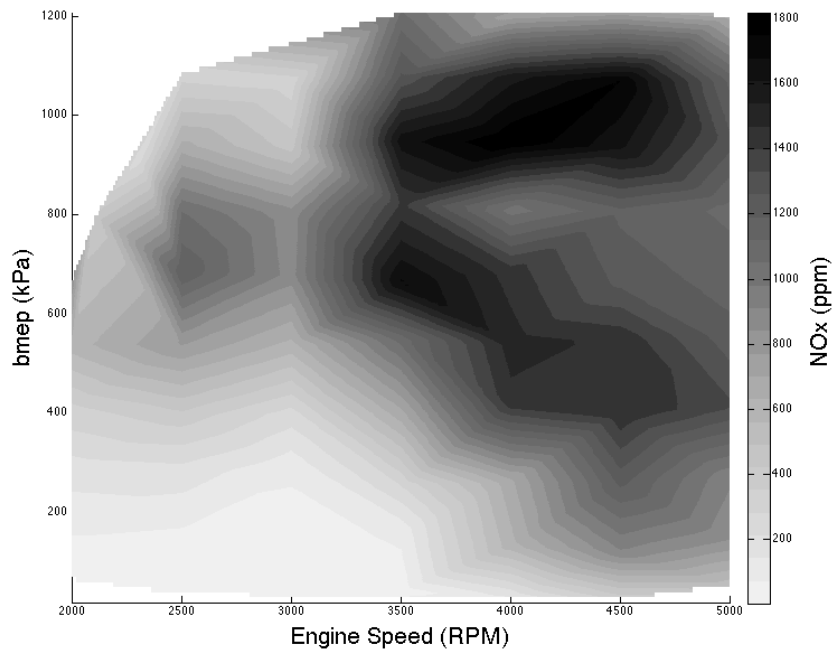


Figure 52 - Gasoline measured NO_x concentrations contour map

Figures 53, 54, and 55 illustrate the natural gas interpolated contour maps for specific NO_x emissions, the NO_x emissions index, and the directly measured NO_x concentrations. For all three emissions parameters, a localized maximum was recognized around engine speeds of 3500 rpm and near a mean effective pressure of 837 kPa. Interestingly, as opposed to gasoline, the specific NO_x emissions do not reflect a globally peak values at any of the testing range limits. In general, NO_x emissions parameters increased with increasing engine speed until speeds of 3500 rpm and then began to decrease with increasing engine speed. The NO_x emissions parameters shared a similar trend to gasoline for the relation of NO_x emissions to mean effective pressures with generally increasing values until approximately 70-90% of full-throttle, followed by a decline in all emissions parameters at higher loads.

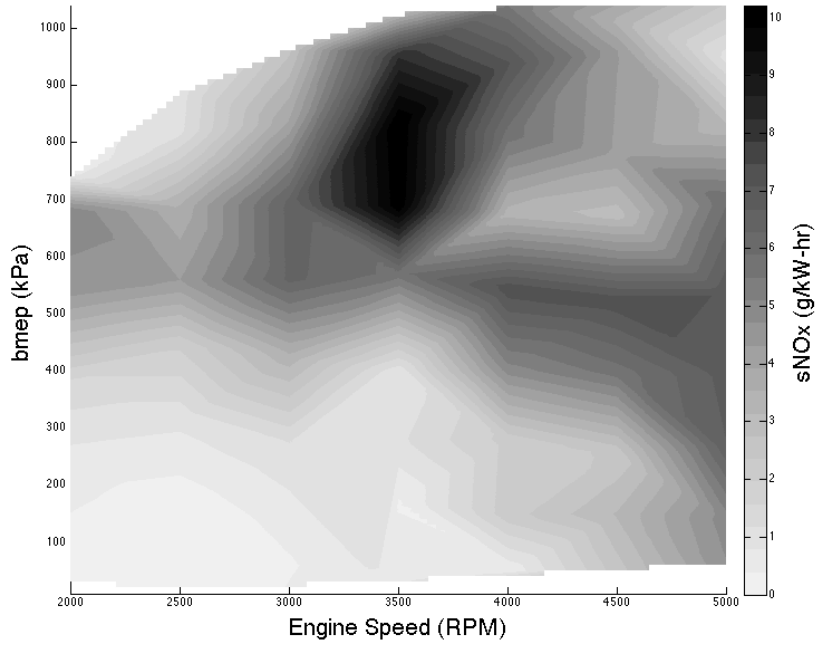


Figure 53 - Natural gas specific NO_x emissions contour map

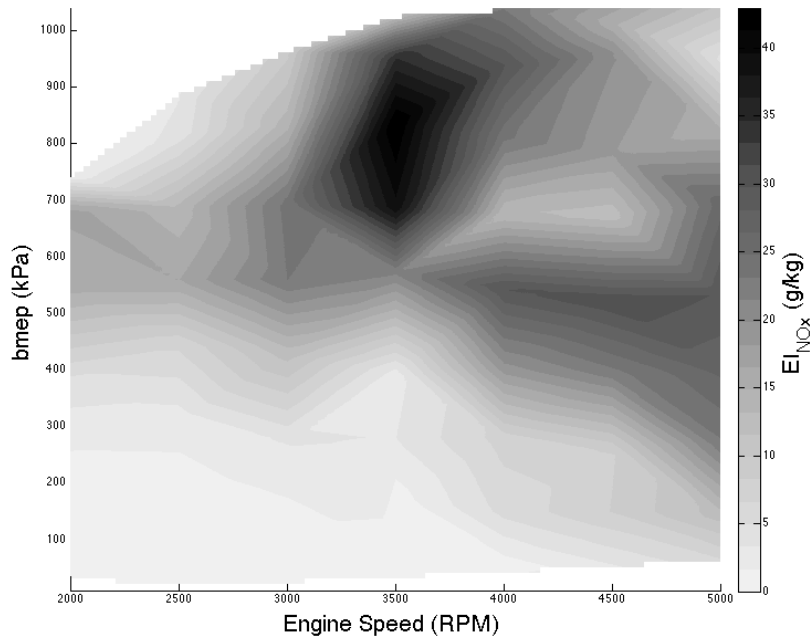


Figure 54 - Natural gas NO_x emissions index contour map

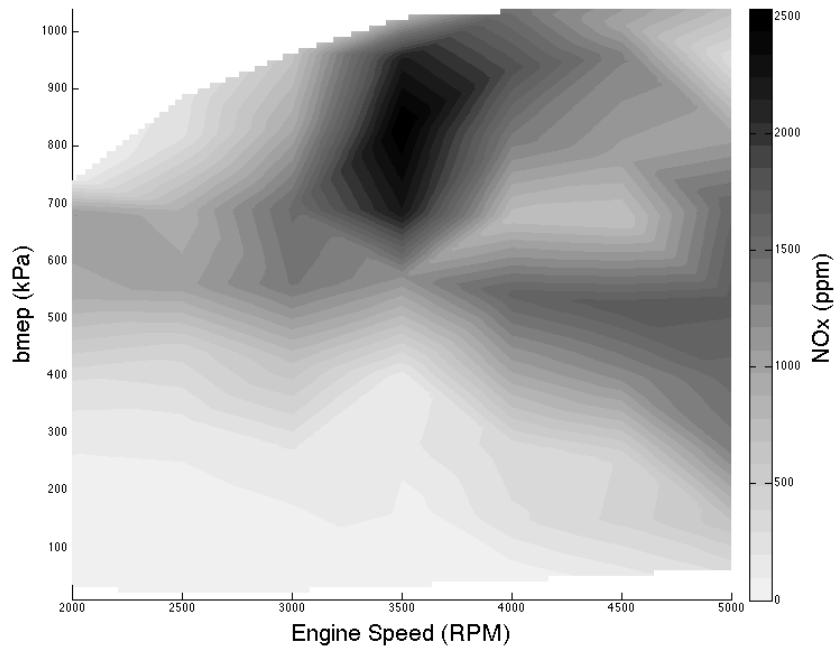


Figure 55 - Natural gas measured NO_x concentrations contour map

A comparison of the NO_x emissions parameters values between gasoline and natural gas proposed inconsistencies between the individual parameters with respect to the fuel used. The maximum specific NO_x values of 13.0 g/kW-hr and 10.3 g/kW-hr for gasoline and natural gas, respectively, indicated a reduction in peak values of 21% for natural gas use. However, the determined average sNO_x values of 3.49 g/kW-hr for gasoline and 3.53 g/kW-hr for natural gas actually indicated about a 1.3% increase in average sNO_x values across all measured conditions. Interestingly, the measured NO_x concentrations resulted in opposite results for the average and maximum value comparisons. A 28% increase in maximum measured NO_x concentrations for natural gas operation was reported with a maximum gasoline concentration of 1841 ppm and a maximum natural gas concentration of 2550 ppm.

However, a 4% reduction in average NO_x concentration for natural gas operation was observed with an average gasoline concentration of 804 ppm and natural gas concentration of 773 ppm. The emissions index comparison differed still from the other NO_x emissions parameters in that a substantial increase in both the maximum and average emissions index values for natural gas use. An increase of 43% in maximum NO_x emissions index values for natural gas use was determined with a maximum gasoline NO_x emissions index of about 24.7 g/kg and a maximum natural gas NO_x emissions index of about 43.3 g/kg. The average gasoline emissions index was determined as 10.4 g/kg, and the average natural gas emissions index was found as 13.2 g/kg, which indicated a 21% increase in the average NO_x emissions index for the use of natural gas against gasoline.

A further examination of the emissions parameters was conducted through the comparison of the specific emissions and emissions index values for gasoline and natural gas over the mean effective pressure range for a fixed engine speed. The respective data was sampled from both test fuels for a fixed engine speed of 2500 rpm. Figures 56, 57, and 58 illustrate the comparisons of the emissions parameters for HC, CO, and NO_x for the test fuels. For both the specific hydrocarbon emissions and HC emissions index, comparative values at mean effective pressures below 300 kPa were observed, but as the engine load increased, the natural gas parameters remained relatively constant or slightly decrease while the gasoline parameters diverged from the natural gas values and non-linearly increased with increasing throttle. The specific CO emissions and CO emissions index indicated that for bmep values below about 575 kPa, natural gas values were considerably less than gasoline values for both the sCO and EI_{CO} parameters but became consistently greater than gasoline

values for mean effective pressures above 575 kPa. For the sNO_x and EI_{NO_x} parameters, both fuels appear to be unimodal across the bmep range. The maximum gasoline sNO_x and EI_{NO_x} values occurred at a bmep of 682 kPa while the maximum natural gas values occurred at 558 kPa. While the peak natural gas value was greater than the gasoline value for both parameters, the gasoline sNO_x and EI_{NO_x} values were observed to generally be lower than natural gas values outside of the parameter ranges.

The dependence on the normalization factor used in the NO_x emissions parameters potentially points to influencers in NO_x formation. As examined in [8], one such influence that could explain the increased NO_x formation at times of natural gas over gasoline could be the greater oxygen concentrations contained in the leaner air-fuel mixtures that the natural gas could achieve. These higher oxygen concentrations could provide a source of oxygen that could increase the NO_x formation rates and total emissions concentrations. However, since the NO_x emissions parameters do not indicate that natural gas consistently produced higher NO_x emissions across the entire operating range, the higher oxygen concentrations of the leaner natural gas mixtures may not entirely account for the NO_x formation. According to [8], for natural gas and gasoline operating under similar compression ratios, natural gas operation could produce lower NO_x emissions due to lower combustion temperatures. Therefore, both the influence of higher oxygen concentrations in fuel-lean natural gas concentrations and the lower natural gas combustion temperatures could explain the observed NO_x formation behavior. This is further supported as Korakianitis indicates that the higher oxygen concentrations will only offset the lower combustion temperatures up to an air-fuel equivalence ratio of about 1.1 [8].

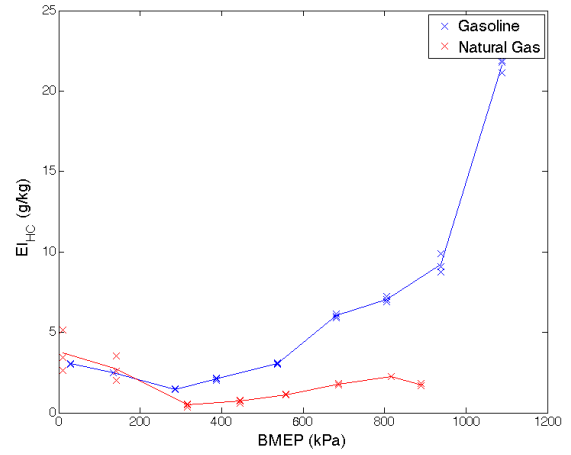
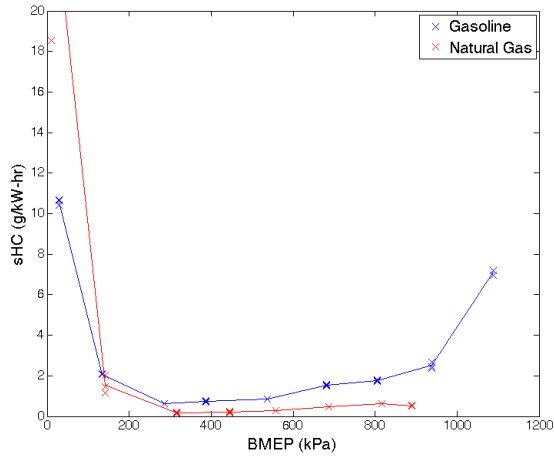


Figure 56 – HC specific emissions (left) and emissions index (right) comparisons at 2500 rpm

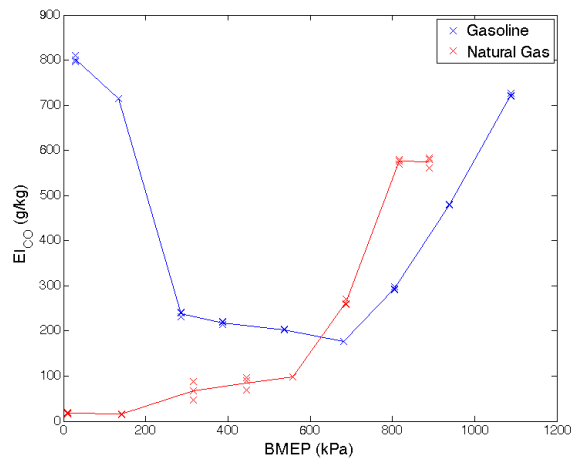
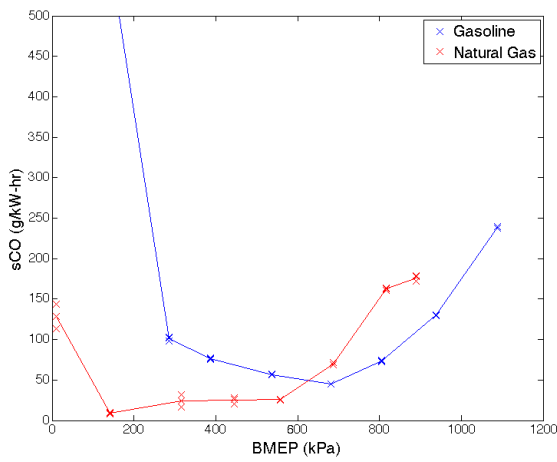


Figure 57 - CO specific emissions (left) and emissions index (right) comparisons at 2500 rpm

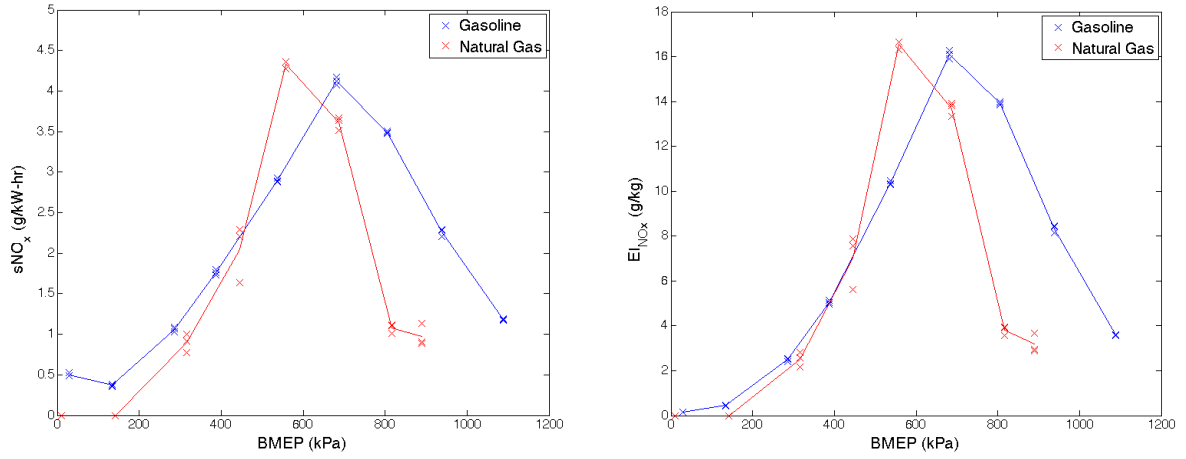


Figure 58 - NO_x specific emissions (left) and emissions index (right) comparisons at 2500 rpm

4 CONCLUSIONS

Natural gas is considered a promising alternative to gasoline as a primary fuel source for internal combustion engines due to its abundant availability, low costs, and decreased pollutant engine emissions. Integration of natural gas into automobile engines could potentially aide manufactures in the development of future engines that are able to meet increasingly stringent regulations on engine emissions and the increasing scarcity and cost of gasoline. This work examined efforts to convert a commonly used gasoline outboard boat motor to run on natural gas. The results compare many of the parameters used to gauge engine performance and provide a valuable beginning towards the potential implementation of natural gas in the marine engine market. Study conclusions can be summarized as follows:

- (1) Conversion of the naturally aspirated engine to natural gas from gasoline resulted in a decrease in the peak engine torque (15% reduction) and a larger decrease in engine power output (21% reduction). The final SAE corrected engine ratings were for 187 kW (251 hp) at 5750 rpm for gasoline and 147 kW (197 hp) at 5100 rpm. Volumetric efficiency losses due to fuel density are assumed as a primary source of the engine performance reductions when operating on natural gas.
- (2) The overall air-fuel equivalence ratio range for gasoline was much shorter than that of natural gas and heavily shifted to rich mixture ratios (between 0.75 and 1). The natural gas equivalence ratio range was dispersed about a larger range of rich and lean conditions (between 0.88 and 1.28).
- (3) It was observed that CO₂ concentrations were considerably reduced (24%) when the test fuel was changed from gasoline to natural gas. For all coinciding natural gas and

gasoline equivalence ratios, the measured excess oxygen concentrations were roughly equivalent. The lean mixture conditions experienced by natural gas allowed for the measurement much greater concentrations of excess oxygen than the maximum gasoline concentrations.

- (4) Comparing the brake specific fuel consumption determined the natural gas fuel consumption was generally around 30 g/kW-hr less than that of gasoline across all operating conditions. The best operating point for gasoline was determined occur at an engine speed of 4000 rpm and near a mean effective pressure of 950 kPa (90% throttle). The natural gas best operating point was found to be at 5000 rpm and near 1048 kPa (full-throttle).
- (5) The comparison of fuel conversion efficiency indicated that gasoline tended to provide higher fuel conversion efficiencies between intermediate power ranges (30-100 kW), but the peak natural gas efficiency was found to be about 0.5% higher than the peak gasoline efficiency.
- (6) The peak gasoline adiabatic flame temperature was found to be nearly 60 K greater than the peak natural gas value. A rich shifting of the peak adiabatic flame temperature was evident for natural gas due to the extended equivalence ratio range. Based on previous research, it was proposed that this is primarily due to a reduction of heat release rate in the lean mixture conditions due to increased product dissociation for hydrocarbons.
- (7) In general, unburned hydrocarbon emissions were found to decrease when the operating fuel was switched from gasoline to natural gas. Average measured HC concentrations

were found to decrease considerably (78%) across the operating range. For the additional normalized emissions parameters, natural gas values were found to moderately decrease (51%) for sHC emissions and significantly decrease (71%) for the HC emissions indexes.

- (8) Average measured CO concentrations were found to greatly decrease (89%) when the test fuel was changed from gasoline to natural gas. Similarly, the average specific CO emissions and EI_{CO} were found to considerably decrease (82% and 78%, respectively).
- (9) Comparative NO_x emissions performance outcomes were found to be dependent on the normalization factor. The measured concentrations were found to increase in maximum concentrations (28% increase) and decrease in average concentrations (4% decrease) when changing from gasoline to natural gas. However, specific NO_x emissions were found to decrease in maximum values (21% reduction) and increase in average s NO_x values (1.3% increase). Also, the NO_x emissions index values were found to both significantly increase for the determined maximum values (43% increase) as well as for the determined average values (21% increase) when switching from gasoline to natural gas.
- (10) The comparison of the NO_x emissions parameters between the two fuels operating on a similar compression ratio indicates a relationship between the presence of higher levels of oxygen in the leaner air-fuel mixtures for natural gas to increase NO_x formation and the lower combustion temperatures for natural gas to decrease NO_x formation that is governed primarily by the air-fuel ratio.

(11) When compared over a fixed engine speed, gasoline HC emissions parameters were found to be greater than natural gas value above low engine loads (300 kPa). Below a mean effective pressure of about 575 kPa, the natural gas CO emissions parameters were found to be less than those of gasoline, but as loads increased, the natural gas CO emissions parameters were found to be greater than those of gasoline. The maximum natural gas NO_x emissions parameters values were found to be greater than the maximum gasoline values and to occur at lower engine loads. For operating conditions outside of the peak natural gas values, natural gas NO_x emissions parameters were found to be generally less than gasoline parameter values at the same condition.

6 REFERENCES

- [1] J. Kjärstad and F. Johnsson, “Resources and future supply of oil,” *Energy Policy*, vol. 37, no. 2, pp. 441–464, Feb. 2009.
- [2] M. J. Economides and D. a. Wood, “The state of natural gas,” *J. Nat. Gas Sci. Eng.*, vol. 1, no. 1–2, pp. 1–13, Jul. 2009.
- [3] M. J. Economides, P. E. Lewis, and R. E. Oligney, “U.S. natural gas in 2011 and beyond,” *J. Nat. Gas Sci. Eng.*, vol. 8, pp. 2–8, Sep. 2012.
- [4] “U.S. Energy Information Administration: Henry Hub Gulf Coast Natural Gas Spot Price.” [Online]. Available: <http://www.eia.gov/dnav/ng/hist/rngwhhdd.htm>. [Accessed: 25-Nov-2013].
- [5] “U.S. Energy Information Administration: New York Harbor Conventional Gasoline Regular Spot Price FOB.” [Online]. Available: http://www.eia.gov/dnav/pet/hist/LeafHandler.ashx?n=PET&s=EER_EPMRU_PF4_Y35NY_DPG&f=D. [Accessed: 25-Nov-2013].
- [6] L. Dondero and J. Goldemberg, “Environmental implications of converting light gas vehicles: the Brazilian experience,” *Energy Policy*, vol. 33, no. 13, pp. 1703–1708, Sep. 2005.
- [7] H. M. Cho and B.-Q. He, “Spark ignition natural gas engines—A review,” *Energy Convers. Manag.*, vol. 48, no. 2, pp. 608–618, Feb. 2007.
- [8] T. Korakianitis, a. M. Namasivayam, and R. J. Crookes, “Natural-gas fueled spark-ignition (SI) and compression-ignition (CI) engine performance and emissions,” *Prog. Energy Combust. Sci.*, vol. 37, no. 1, pp. 89–112, Feb. 2011.
- [9] K. Zeng, D. Jiang, J. Wang, L. Liu, B. Liu, Y. Ren, and Z. Huang, “Combustion characteristics of a direct-injection natural gas engine under various fuel injection timings,” *Appl. Therm. Eng.*, vol. 26, no. 8–9, pp. 806–813, Jun. 2006.
- [10] S. Shiga, H. Nakamura, N. Jingu, S. Ozone, Z. Huang, M. Kono, T. Karasawa, M. Tsue, H. T. C. Machacon, and T. Ueda, “A study of the combustion and emission characteristics of compressed-natural-gas direct-injection stratified combustion using a rapid-compression-machine,” *Combust. Flame*, vol. 129, no. 1–2, pp. 1–10, 2002.
- [11] M. Rink, G. Eigenberger, and U. Nieken, “Heat-Integrated Exhaust Purification for Natural Gas Engines,” *Chemie Ing. Tech.*, vol. 85, no. 5, pp. 656–663, May 2013.

- [12] F. Ma, H. Liu, J. Wang, S. Zhao, Y. Li, and Y. Wang, “Experimental study on thermal efficiency and emission characteristics of a lean burn hydrogen enriched natural gas engine,” *Int. J. Hydrogen Energy*, vol. 32, no. 18, pp. 5067–5075, Dec. 2007.
- [13] A. Mariani, M. V. Prati, A. Unich, and B. Morrone, “Combustion analysis of a spark ignition i. c. engine fuelled alternatively with natural gas and hydrogen-natural gas blends,” *Int. J. Hydrogen Energy*, vol. 38, no. 3, pp. 1616–1623, Feb. 2013.
- [14] P. H. Barros Zárante and J. R. Sodr e, “Evaluating carbon emissions reduction by use of natural gas as engine fuel,” *J. Nat. Gas Sci. Eng.*, vol. 1, no. 6, pp. 216–220, Dec. 2009.
- [15] K. Kobayashi, S. Yoshimi, T. Sako, S. Kanematsu, H. Ohtsubo, T. Nakazono, S. Morimoto, and K. Suzuki, “Development of HCCI natural gas engines,” *J. Nat. Gas Sci. Eng.*, vol. 3, no. 5, pp. 651–656, Oct. 2011.
- [16] Yamaha, “F250 Specifications.” [Online]. Available: http://yamahaoutboards.com/outboards/V6-3_3L/specifications. [Accessed: 12-Dec-2013].
- [17] Land-and-Sea, “DYNOMite Owner’s Manual.” .
- [18] “Infrared Industries: FGA4000XDS Specifications.” [Online]. Available: <http://www.infraredindustries.com/product/fga4000xds-gas-analyzer/>. [Accessed: 29-Nov-2013].
- [19] J. B. Heywood, *Internal Combustion Engine Fundamentals*, 1st ed. McGraw-Hill, Inc., 1988, p. 46.
- [20] Unitrove, “Natural Gas Density Calculator.” [Online]. Available: <http://www.unitrove.com/engineering/tools/gas/natural-gas-density>. [Accessed: 13-Dec-2013].
- [21] K. K. Kuo, *Principles of Combustion*, 2nd ed. Hoboken, New Jersey: John Wiley & Sons, Inc., 2005, p. 701.
- [22] L. F. Khilyuk, G. V. Chilingar, J. O. Robertson, and B. Endres, *Gas Migration*. Elsevier Inc., 2000, pp. 238–240.
- [23] “Lower and Higher Heating Values of Gas, Liquid and Solid Fuels,” in in *Biomass Energy Data Book*, 4th ed., .

- [24] Unitrove, "Natural Gas Calorific Value Calculator." [Online]. Available: <http://www.unitrove.com/engineering/tools/gas/natural-gas-calorific-value>. [Accessed: 14-Dec-2013].
- [25] C. Law, a Makino, and T. Lu, "On the off-stoichiometric peaking of adiabatic flame temperature," *Combust. Flame*, vol. 145, no. 4, pp. 808–819, Jun. 2006.

APPENDIX

Test procedures for the experiment were split between procedures for measuring engine power and engine exhaust. The specific procedure was slightly different for each measurement type depending on the fuel source. The following sections indicate the specific procedures used throughout experimentation.

Test Cell Preparation

The following steps were performed before any of the testing procedures described in later sections were performed.

1. Connect dynamometer load valve, natural gas ECM (if applicable), and engine battery [+] wires to the [+] terminal of the 12VDC marine engine battery.
2. Connect dynamometer load valve, dynamometer ground, natural gas ECM (if applicable), and engine battery [-] wires to the [-] terminal of the 12VDC marine engine battery.
3. If applicable, ensure the exhaust sample probe is inserted into the engine exhaust manifold.
4. Trim the engine up and move the engine into the exhaust shroud.
5. Connect the drain and feed water input lines to the water-brake absorber.
6. Insert the appropriate restrictor in the feed water outlet of the water-brake absorber and connect the feed water outlet line to the water-brake absorber.
7. Trim the engine down and enclose the engine in the exhaust shroud.
8. If applicable, open the natural gas tank and enable flow to the pressure reducer.

9. If applicable, ensure engine quick connectors and natural gas tank quick connectors are connected to the control system.
10. Start the desktop computer.
11. Connect the RPM pickup and torque load cell to the data computer.
12. Connect the auto load valve servo power to the data computer.
13. Plug the power input into the data computer and connect the data computer USB to the desktop computer.
14. Start the DYNO-MAX Pro software.
15. If applicable, start the natural gas controller software.
16. Open any valves in the dynamometer feed water supply system to allow flow through the system.
17. If applicable, turn on the natural gas pressure reducer warming water pump.
18. Turn on the dynamometer feed water pump.
19. Turn on the exhaust removal system.
20. Continue to one of the following sections for testing procedures.

Gasoline Power Sweep Measurements

The following steps were performed when taking engine power measurements via a swept-RPM automated test for an engine running on gasoline.

1. Fill the gas tank with minimum 89-octane rating with no ethanol gasoline.
2. Prime the engine fuel line using the priming bulb.
3. Open a new run in the DYNO-MAX Pro software.

4. Change the software view to the console view.
5. Right click and select “Configure DYNOMite Controls.”
6. Set the appropriate Gain, Drift, and Rate values.
 - a. For gasoline engine control, the a setting of Gain=8, Drift=8, and Rate=8 was used to control the engine.
7. Click “OK.”
8. Right click and select “Edit Automated-Test Setup.”
9. Select the start and end RPM values of the test.
 - a. The NCSU laboratory began the test at 2500 RPM and ended the test at 5700 RPM.
10. Ensure the “linear sweep rate” is checked and set the acceleration rate to “400 RPM/second.”
11. Click “OK.”
12. On the console screen, press the “Auto” button.
13. Turn on the engine via the key on the engine control unit.
14. In the DYNO-MAX Pro software, right click and select “Calibrate DYNOMite Channels.”
15. Select the “Torque” tab.
16. Select “Zero.”
17. Click “OK.”
18. Wait for the engine RPM to slow and stabilize.
19. Put the engine in gear using the engine control unit.

20. Gradually accelerate using the engine control unit until the engine is at full throttle.
21. Click “Run Auto Test.”
22. Wait for the automated test to complete.
23. When the test is complete, gradually decelerate the engine back to idle.
24. Turn off the engine.
25. Press “save.”
26. In the comments box, note the ambient air temperature, pressure, and humidity.
27. View the horsepower and torque curves by selecting the plot option (F5) in the
DYNO-MAX Pro software.

Gasoline Exhaust Measurements

The following steps were performed when taking engine exhaust measurements for an engine running on gasoline.

1. Turn on the fuel scale.
2. Turn on the exhaust gas analyzer. The analyzer may take up to five minutes to warm up and zero.
3. If connected, disconnect the exhaust gas sampling probe line from the exhaust gas analyzer.
4. Fill the gas tank with minimum 89-octane rating with no ethanol gasoline.
5. Prime the engine fuel line using the priming bulb.
6. Open a new run in the DYNO-MAX Pro software.
7. Change the software view to the console view.

8. Right click and select “Configure DYNOMite Controls.”
9. Set the appropriate Gain, Drift, and Rate values.
 - a. For gasoline engine control, the NCSU laboratory found a setting of Gain=8, Drift=8, and Rate=8 to adequately control the engine.
10. Click “OK.”
11. On the console screen, press the “Hold” button.
12. Using the arrow keys, set the hold RPM for which exhaust measurements will be taken.
13. Turn on the engine via the key on the on the engine control unit.
14. In the DYNO-MAX Pro software, right click and select “Calibrate DYNOMite Channels.”
15. Select the “Torque” tab.
16. Select “Zero.”
17. Click “OK.”
18. Wait for the engine RPM to slow and stabilize.
19. Press “measure” on the exhaust gas analyzer.
20. Connect the exhaust gas sampling probe line to the exhaust gas analyzer.
21. Put the engine in gear using the engine control unit.
22. Using the engine control unit, gradually accelerate until the engine reaches the hold RPM and the reported engine load is close to 0 ft-lbs (approximately less than 5 ft-lbs).
23. Record the torque reading.

24. Record the RPM reading.
25. Using a timer, watch the fuel scale reading and note the time, Δt , it takes for the fuel mass to decrease an appropriate amount, Δm .
 - a. Δm should be chosen relative to how quickly the engine is consuming fuel.
The operator should choose a Δm that allows for accurate timing over the chosen value. Small Δm values may produce small and inconsistent Δt values.
The NCSU laboratory commonly used Δm values of 10, 20, and 30 grams.
26. Record Δm and Δt .
27. Press “hold” on the exhaust gas analyzer to hold the analyzer values.
28. Record HC, CO, CO₂, O₂, NO_x, and AFR values from the exhaust gas analyzer.
29. Press “hold” on the exhaust gas analyzer to release the analyzer values.
30. Repeat steps 27 through 29 twice more.
31. Record the ambient air temperature, absolute pressure, and humidity measurements.
32. Using the engine control unit, increase the throttle until the engine load increases by a predetermined ΔLoad .
 - a. ΔLoad should be an adequately sized value based on the expected range of load values from minimum to maximum throttle positions that produces enough data points to recognize exhaust trends. The NCSU laboratory found ΔLoad values of 25 ft-lbs to provide consistent results for the indicated Yamaha F250 engine.
 - b. The full throttle load data point does not need to be greater than the previous point by ΔLoad .

33. Repeat steps 23 through 31 for this load value.
34. Repeat step 32 and 33 until exhaust gas values have been recorded for the engine at full throttle.
35. Gradually decelerate the engine to idle.
36. Turn off the engine.
37. For complete engine exhaust testing, repeat steps 12 through 36 and adjusting the hold RPM in step 12 by a determined Δ RPM value.
 - a. The NCSU laboratory used Δ RPM values of 500 RPM from 2000 RPM to 5500 RPM to produce an adequate map of the engine exhaust characteristics.

Natural Gas Power Sweep Measurements

The following steps were performed when taking engine power measurements via a swept-RPM automated test for an engine running on natural gas.

1. Fill the gas tank with minimum 89-octane rating with no ethanol gasoline.
2. Prime the engine fuel line using the priming bulb.
3. In the natural gas software, set the natural gas switch-over RPM.
 - a. The switch-over RPM should be 500-100 RPM less than the beginning RPM value of the automated sweep test.
4. Open a new run (F12) in the DYNO-MAX Pro software.
5. Change the software view to the console view (F11).
6. Right click and select “Configure DYNomite Controls.”
7. Set the appropriate Gain, Drift, and Rate values.

- a. For natural gas engine control, the NCSU laboratory found a setting of Gain=8, Drift=1, and Rate=7 to adequately control the engine.
 - b. These values may need to be adjusted depending of water supply configurations and engine capabilities.
8. Click “OK.”
9. Right click and select “Edit Automated-Test Setup.”
10. Select the start and end RPM values of the test.
 - a. The NCSU laboratory began the test at 2500 RPM and ended the test at 5700 RPM.
11. Ensure the “linear sweep rate” is checked and set the acceleration rate to “400 RPM/second.”
12. Click “OK.”
13. On the console screen, press the “Auto” button.
14. Turn on the engine via the key on the engine control unit.
15. In the DYNO-MAX Pro software, right click and select “Calibrate DYNOMite Channels.”
16. Select the “Torque” tab.
17. Select “Zero.”
18. Click “OK.”
19. Wait for the engine RPM to slow and stabilize.
20. Put the engine in gear using the engine control unit.

21. Gradually accelerate using the engine control unit until the engine reaches the natural gas switch-over RPM.
22. Ensure the engine is now running on natural gas.
23. Continue gradually accelerating using the engine control unit until the engine is at full throttle.
24. Click “Run Auto Test.”
25. Wait for the automated test to complete.
26. When the test is complete, decelerate the engine back to idle.
27. Turn off the engine.
28. Press “save.”
29. In the comments box, note the ambient air temperature, pressure, and humidity.
30. View the horsepower and torque curves by selecting the plot option in the DYNO-MAX Pro software.

Natural Gas Exhaust Measurements

The following steps were performed when taking engine exhaust measurements for an engine running on natural gas.

1. Turn on the natural gas flow rate meter.
2. Turn on the exhaust gas analyzer. The analyzer may take up to five minutes to warm up and zero.
3. If connected, disconnect the exhaust gas sampling probe line from the exhaust gas analyzer.

4. Fill the gas tank with gasoline and place it on the fuel scale.
 - a. For the indicated Yamaha F250 a minimum 89-octane rating with no ethanol is specified from the manufacturer.
5. Prime the engine fuel line using the priming bulb.
6. In the natural gas software, set the natural gas switch-over RPM.
 - a. The switch-over RPM should be 500-100 RPM less than the hold RPM value of the exhaust test.
7. Open a new run (F12) in the DYNO-MAX Pro software.
8. Change the software view to the console view (F11).
9. Right click and select “Configure DYNOmite Controls.”
10. Set the appropriate Gain, Drift, and Rate values.
 - a. For natural gas engine control, the NCSU laboratory found a setting of Gain=8, Drift=1, and Rate=7 to adequately control the engine.
11. Click “OK.”
12. On the console screen, press the “Hold” button.
13. Using the arrow keys, set the hold RPM for which exhaust measurements will be taken.
14. Turn on the engine via the key on the on the engine control unit.
15. In the DYNO-MAX Pro software, right click and select “Calibrate DYNOmite Channels.”
16. Select the “Torque” tab.
17. Select “Zero.”

18. Click “OK.”
19. Wait for the engine RPM to slow and stabilize.
20. Press “measure” on the exhaust gas analyzer.
21. Put the engine in gear using the engine control unit.
31. Gradually accelerate using the engine control unit until the engine reaches the natural gas switch-over RPM.
32. Ensure the engine is now running on natural gas.
22. Connect the exhaust gas sampling probe line to the exhaust gas analyzer.
23. Using the engine control unit, continue gradually accelerating until the engine reaches the hold RPM and the reported engine load is close to 0 ft-lbs (approximately less than 5 ft-lbs).
24. Record the torque reading.
25. Record the RPM reading.
26. Record the flow rate meter reading.
27. Record the natural gas map pressure reading from the natural gas software.
28. Record the natural gas temperature reading from the natural gas software.
29. Press “hold” on the exhaust gas analyzer to hold the analyzer values.
30. Record HC, CO, CO₂, O₂, NO_x, and AFR values from the exhaust gas analyzer.
31. Press “hold” on the exhaust gas analyzer to release the analyzer values.
32. Repeat steps 31 through 33 twice more.
33. Record the ambient air temperature, absolute pressure, and humidity measurements.

34. Using the engine control unit, increase the throttle until the engine load increases by a predetermined Δ Load.
 - a. Δ Load should be an adequately sized value based on the expected range of load values from minimum to maximum throttle positions that produces enough data points to recognize exhaust trends. The NCSU laboratory found Δ Load values of 25 ft-lbs to provide consistent results for the indicated Yamaha F250 engine.
35. Repeat steps 24 through 33 for this load value.
36. Repeat step 34 and 35 until exhaust gas values have been recorded for the engine at full throttle.
37. Gradually decelerate the engine to idle.
38. Turn off the engine.
39. For complete engine exhaust testing, repeat steps 13 through 38 and adjusting the hold RPM in step 13 by a determined Δ RPM value.
 - a. The NCSU laboratory used Δ RPM values of 500 RPM from 2000 RPM to 5500 RPM to produce an adequate map of the engine exhaust characteristics.